Check for updates

SEDIMENTOLOGY the journal of the International Association of Sedimentologists IAS

Sedimentology (2026) **73**, 2081–2119 doi: 10.1111/sed.70126

Spatial and temporal evolution of a coastal erg margin: The Middle Jurassic Page Sandstone, southern Utah, USA

VICTOR J. P. HÊME DE LACOTTE*, CHESTER H. C. DAVIES*, BRIONY J. BOWLER*, STUART M. CLARKE* and THOMAS J. H. DODD*,†
*Basin Dynamics Research Group, School of Life Sciences, Keele University, Keele, Staffordshire ST5 5BG, UK (E-mail: v.j.p.heme.de.lacotte@keele.ac.uk)
†British Geological Survey, Lyell Centre, Research Avenue South, Edinburgh EH21 6ER, UK

Associate Editor: Jean-Yves Reynaud

ABSTRACT

Aeolian deflationary events are erosive to static stages where sediment supply is insufficient to support bedform migration and preservation in the rock record. In the vicinity of shallow-marine environments, inland rises of relative water table and associated generation of deflationary super surfaces may be driven by the onset of transgression phases. However, despite this link being widely recognised in ancient systems, current genetic models for coastal erg margins fail to account for stratigraphical complexities and spatial changes in aeolian sedimentary architectures across their different depositional belts. This study addresses this gap by investigating the spatio-temporal evolution of the Middle Jurassic Temple Cap Formation and Page Sandstone and their relationship with the contemporaneous shallow-marine strata of the Carmel Formation, in southern Utah, USA. A set of twenty observed lithofacies grouped into eight architectural elements were identified in seven sedimentary logs and four outcrop panels collected across two palaeoshoreline-perpendicular transects. Spatio-temporal analysis of the documented stratigraphical framework reveals two major erg-building phases, each interpreted as the product of a regressive system tract, and intercalated with intervening transgressive marine system tracts. Depositional models incorporating geometries of aeolian architectural elements and their relationships with marine units are proposed for both regressive and transgressive scenarios. Regressive system tracts are dominated by superimposed draa cosets in coastal erg centre environments that grade laterally into simple transverse bedform sets as sediment availability decreases towards marginal regions. Transgressive system tracts are, conversely, the scene of significant sediment remobilisation through tidal ravinement in erg margin regions and regional deflationary super surface development further inland. Detailed documentation of sedimentary architecture within aeolian–marine sequences, and investigation of the variable expression of their bounding surfaces, helps constraining the depositional record of these complex systems. Exploring the interplay between aeolian and marine processes and their associated stratigraphical products improves our ability to populate reservoir models and predict facies distribution in analogous subsurface systems.

Keywords aeolian deflation, Carmel Formation, coastal erg margin, Page Sandstone, Utah.

© 2026 The Author(s). *Sedimentology* published by John Wiley & Sons Ltd on behalf of International Association of Sedimentologists.
This is an open access article under the terms of the Creative Commons Attribution License, which permits use, distribution and reproduction in any medium, provided the original work is properly cited.

INTRODUCTION

Coastal erg systems develop under arid to semi-arid climatic settings in regions where sediment availability is sufficient to enable aeolian bedform development and migration. They represent a style of erg margin characterised by regular deflations of the dune field that are related to marine flooding events from bordering paralic and shallow-marine environments (Corbett, 1993; Havholm & Kocurek, 1994; Cross *et al.*, 2023). As a consequence, the recognition of coastal aeolian systems is based upon systematic seaward sedimentological variations across the margin, including (i) a decrease in aeolian bedform complexity and size; (ii) a decrease in dune crest-line sinuosity; and (iii) an increase in the occurrence of evaporitic sabkha and supratidal deposits, as evidenced in studies of both modern settings (e.g. Inman *et al.*, 1966; Fryberger *et al.*, 1983, 1988, 1990; Kocurek *et al.*, 1992; Rivers *et al.*, 2020) and ancient strata (e.g. Dott *et al.*, 1986; Kamola & Chan, 1988; Jordan & Mountney, 2012; Rodríguez-López *et al.*, 2012; Polo *et al.*, 2020; Pettigrew *et al.*, 2021). These studies suggest that coastal erg-building sequences are controlled in part by fluctuations in relative sea-level, and therefore, their key bounding surfaces may be genetically linked to marine flooding surfaces of stratigraphical significance (Blakey *et al.*, 1996; Rodríguez-López *et al.*, 2013). Similarly to upstream-controlled fluvially dominated settings (cf. Shanley & McCabe, 1994), large-scale sequence-stratigraphical models have previously associated the development and accumulation of coastal aeolian strata with the deposition of Lowstand Systems Tracts (LST) (Veiga *et al.*, 2005; Blanchard *et al.*, 2016; Vieira & dos Santos Scherer, 2017), which is then followed by transgression-induced erg termination within basins occurring under arid climates (Strömbäck *et al.*, 2005; Paz *et al.*, 2021). Climatic cyclicity models for arid continental depositional systems provide means of correlating wetting- and drying-upward system tracts, as well as associated points of maximum aridity and humidity, between vertical successions (Howell & Mountney, 1997). Although such models highlight the influence of climatically driven variability in sediment supply upon preserved aeolian sedimentary architectures, they do not consider scenarios of non-eustatic relative sea-level fluctuation nor the influence of variation in rates of accommodation creation (Kocurek & Havholm, 1993; Cosgrove *et al.*, 2022) and tectonic setting (Cosgrove *et al.*, 2023). Changes in base-level influence how continental systems behave (e.g. Schumm, 1993), including aeolian systems (Kocurek *et al.*, 1991). Consequently, uncertainties remain regarding the link between the development of aeolian deflationary surfaces (and their associated sequences) and changes in relative sea-level. These uncertainties are compounded by the fact that marginal-erg systems present significant spatial variability in sedimentary architecture across their transitional zones (e.g. Mountney & Jagger, 2004; Mountney, 2006; Jordan & Mountney, 2010; Al-Masrahy & Mountney, 2013; Cross *et al.*, 2023), which may be affected by a complex suite of allogenic forcing mechanisms that complicate their analyses in the rock record.

Marginal-erg systems have received much attention for their potential as good subsurface reservoir targets for long term carbon storage (e.g. Foote *et al.*, 2025; Melnyk *et al.*, 2026). Intraformational baffles and barriers to subsurface fluids in marginal aeolian successions result directly from the interactions between adjacent depositional systems involving sediment mixing and reworking of variable fractions (e.g. Mountney & Jagger, 2004; Taggart *et al.*, 2010; Gross *et al.*, 2023; Priddy *et al.*, 2023; Pettigrew *et al.*, 2024; Bofill *et al.*, 2025). Understanding the driving mechanisms behind the generation of potential heterogeneities in the sediments of aeolian–marine margins is therefore crucial for assessing the associated reservoir potential for subsurface CO_2 storage (e.g. Issautier *et al.*, 2013; Sohal *et al.*, 2021).

Mixed aeolian–marine successions have been recognised and documented in multiple systems across various ages. Early studies of the Cambro-Ordovician succession of the northern Mississippi Valley, USA (Dott *et al.*, 1986) and Palaeozoic to Mesozoic successions of the Paradox Basin, USA (Blakey & Middleton, 1983; Chan & Kocurek, 1988; Kamola & Chan, 1988; Chan, 1989; Atchley & Loope, 1993; Blakey *et al.*, 1996) revealed the co-occurrence of aeolian and marine facies. These studies recognised complex facies interactions between the two depositional systems in the rock record, with comparable processes in modern analogous systems also being well documented (e.g. Fryberger *et al.*, 1990; Rivers *et al.*, 2020). Based upon this evidence, further works investigated the stratigraphical expression of aeolian–marine margins in basins with different depositional scenarios

© 2026 The Author(s). *Sedimentology* published by John Wiley & Sons Ltd on behalf of International Association of Sedimentologists,

13653091, 2026, 6, Downloaded from https://onlinelibrary.wiley.com/doi/10.1111/sed.70126 by British Geological Survey, Wiley Online Library on [15/10/2026]. See the Terms and Conditions (https://onlinelibrary.wiley.com/terms-and-conditions) on Wiley Online Library for rules of use; OA articles are governed by the applicable Creative Commons License

and climatic settings. Detailed analysis of Mesozoic deposits in the Iberian Basin, Spain, revealed complex marginal-erg systems deposited in semi-arid to sub-humid climates, which were affected by ephemeral fluvial systems and marine incursions (Rodríguez-López *et al.*, 2010, 2012; Campos-Soto *et al.*, 2022; Grantham, 2025). These observations from the rock record were compared with the modern Lençóis Maranhenses dune field, Brazil. Comparably, Jordan & Mountney (2010, 2012) demonstrated the complicated stratigraphical arrangements inherited from the intricate competition between fluvial, marine and aeolian systems in the Pennsylvanian–Permian Lower Cutler Beds, Utah, USA. More recent studies have focused upon erg deflation within transgressional relative sea-level scenarios, including studies on the Jurassic Carmel Formation (Hême de Lacotte *et al.*, 2026), the Curtis-Summerville succession of southeast Utah (Zuchuat *et al.*, 2019a; Cross *et al.*, 2023) and the Upper Jurassic to lower Cretaceous Mendoza Group, Neuquén Basin, Argentina (Paz *et al.*, 2021). Together, these studies provide genetic models for marine-aeolian margins incorporating facies diversity and evolution in response to environmental dynamics.

Studies on the Pennsylvanian Amsden and Tensleep formations in Wyoming, USA, proposed sequence-stratigraphical frameworks incorporating aeolian strata within idealised sequences deposited during eustatic fluctuations (Carr-Crabaugh & Dunn, 1996; Blanchard *et al.*, 2016). Despite providing considerable advances, these models for aeolian–marine margins do not fully encapsulate the genetic links between the generation of deflationary super surfaces and variations in relative sea-level. Furthermore, the sequence stratigraphical framework proposed by Blanchard *et al.* (2016) does not consider the results of analysis of successions deposited under ice cap-free phases. Ultimately a generic model for the development of aeolian sequences in coastal settings needs to be framed, regardless of the suite of allogenic controlling factors (which are mostly case-specific parameters).

By building upon the findings of Havholm & Kocurek (1994) and Carr-Crabaugh & Kocurek (1998), this study seeks to fill this gap in understanding through detailed sedimentological analysis of a preserved aeolian–marine margin succession on the Colorado Plateau, USA. This work focusses on the Middle Jurassic Temple Cap Formation and Page Sandstone, a coastal aeolian succession bordering contemporaneous shallow-marine and tidal deposits of the Carmel Formation (Blakey *et al.*, 1983). Such a system can be considered analogous to modern-day coastal dune fields occurring in arid regions, such as the Guerrero Negro barrier island (Fryberger *et al.*, 1990), the Gran Desierto Dune Field, Mexico (Beveridge *et al.*, 2006), or the Khor Al Adaid embayment, Qatar (Rivers *et al.*, 2020). This study presents a spatio-temporal analysis of the aeolian Temple Cap Formation and the overlying intertonguing zone between the aeolian Page Sandstone and the shallow-marine Carmel Formation.

Through this analysis, this study aims to (i) document the sedimentary architecture diversity and relationships between both aeolian and tidal depositional environments; (ii) analyse the spatial variability in the sedimentary expression of aeolian–marine interactions; (iii) recognise regressive and transgressive system tracts and the correlation of their associated stratigraphical surfaces at the basin scale; (iv) demonstrate the genetic links between deflationary super surface generation and marine flooding events in response to allogenic forcings; and (v) propose a generalised model for the spatial complexity of aeolian sequences in response to marine flooding events.

Documenting the sedimentary record of process interactions between aeolian and tidal forces helps decipher the relative roles of autocyclic and allogenic mechanisms upon sediment distribution through the stratigraphical record of ancient aeolian–marine systems. By constraining the sedimentary characteristics of such environments in relation to relative sea-level dynamics, this study puts emphasis on facies distribution and stratigraphical arrangements in analogous subsurface systems.

GEOLOGICAL SETTING

The Temple Cap Formation and Page Sandstone are Middle Jurassic (Aalenian–Bathonian) successions that form the basal lithostratigraphical units of the San Rafael Group of the western USA (Fig. 1B). They represent the evolution of a coastal erg developed in a southward blowing wind system along the shoreline of the Sundance Seaway. These successions were deposited on the southern edge of the Utah-Idaho Trough (Fig. 1A): an elongated retro arc foreland basin that extended across the Colorado Plateau during Jurassic times and was generated by

© 2026 The Author(s). *Sedimentology* published by John Wiley & Sons Ltd on behalf of International Association of Sedimentologists, *Sedimentology*, **73**, 2081–2119

13653091, 2026, 6, Downloaded from https://onlinelibrary.wiley.com/doi/10.1111/sed.70126 by British Geological Survey, Wiley Online Library on [15/10/2026]. See the Terms and Conditions (https://onlinelibrary.wiley.com/terms-and-conditions) on Wiley Online Library for rules of use; OA articles are governed by the applicable Creative Commons License

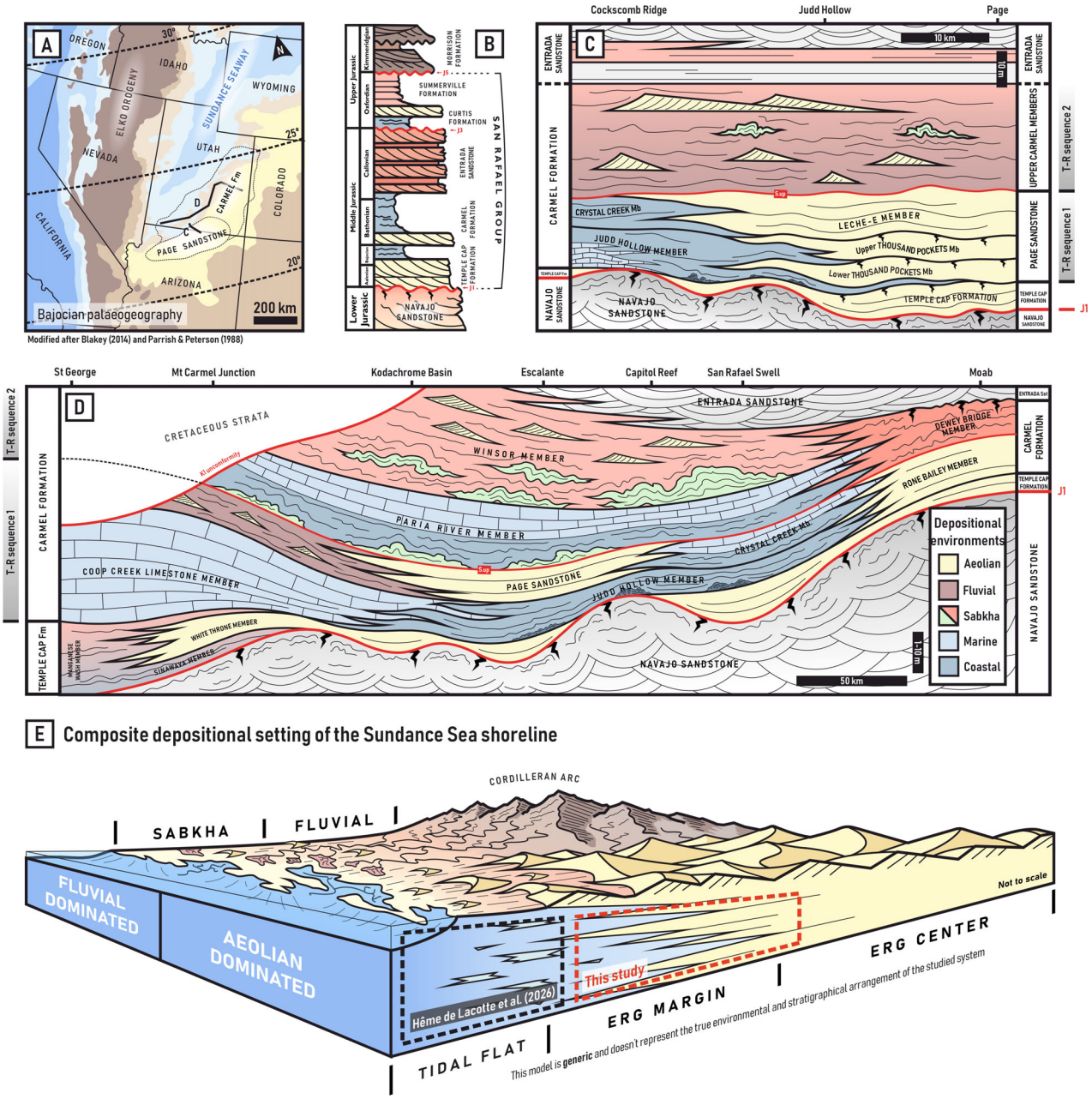

Fig. 1. (A) Palaeogeographical settings of the Colorado Plateau during Bajocian times, adapted from Parrish & Peterson (1988) and Blakey (2014). (B) Schematic stratigraphy of the San Rafael Group. (C, D) Lithostratigraphic framework for the Temple Cap Formation, the Carmel Formation and the Page Sandstone on transects perpendicular (C) and parallel (D) to the Sundance Sea palaeocoastline. (E) Composite depositional setting of the Sundance Sea margin, displaying the variety of depositional environments observed in the San Rafael Group. This work focuses on continental deposits contemporaneous to the shallow-marine succession previously documented by Hême de Lacotte *et al.* (2026).

flexural subsidence in response to Cordilleran nappe stacking (Bjerrum & Dorsey, 1995; Kowallis *et al.*, 2001; Thorman, 2011). Temple Cap and Page successions are exposed across southern Utah and northern Arizona, from Escalante in Utah, to south of Page in Arizona, and were deposited in a northward drifting palaeo-region characterised by intertropical

13653091, 2026, 6, Downloaded from https://onlinelibrary.wiley.com/doi/10.1111/sed.70126 by British Geological Survey, Wiley Online Library on [15/10/2026]. See the Terms and Conditions (https://onlinelibrary.wiley.com/terms-and-conditions) on Wiley Online Library for rules of use; OA articles are governed by the applicable Creative Commons License

climates (Fig. 1A; Kocurek & Dott, 1983). The Page Sandstone grades northward and westward into the tidal sediments of the Carmel Formation, with a complex stratigraphical interplay between the two systems that is illustrated by a subdivision of these strata into twelve composite members (Fig. 1C and D; Blakey *et al.*, 1996). Temple Cap and Page successions onlap southeastward onto the Monument Upwarp, a structural high linked to foreland basin bulging dynamics (Fig. 2; Blakey *et al.*, 1988). Overall, the depositional system represented by the Temple Cap Formation, and the overlying contemporaneous Page Sandstone and Carmel Formation is characterised by significant lateral facies transitions associated with complex interactions between shallow-marine to paralic and arid continental depositional processes (Blakey *et al.*, 1983; Jones & Blakey, 1993, 1997). Their transitional stratigraphical relationships translate the spatial dynamics and temporal evolution of these contemporaneous depositional environments. Together, the Temple Cap-Page-Carmel system represents the depositional record of a coastal erg margin responding to the fluctuation in relative sea-level of the Sundance Sea during an ice sheet-free Jurassic hot house phase (Hallam, 1985). These units present heterogenous detrital zircon age populations comparable to older Jurassic aeolian deposits, suggesting a rejuvenation of previous erg systems (Dickinson & Gehrels, 2009).

Havholm *et al.* (1993) proposed a subdivision of the Page Sandstone into six informal units relating to different correlative architectural assemblages, each of them bounded by regional deflationary super surfaces (Fig. 2). This subdivision corresponds to a lithostratigraphical framework suggested by Blakey *et al.* (1996). However, more recent chronological age analysis from Dickinson *et al.* (2010) suggests that both the Temple Cap and the Page successions are contemporaneous and should thus be treated as a whole system (Doelling *et al.*, 2013; Sprinkel *et al.*, 2024).

The Temple Cap Formation and, where such is not preserved or deposited, the younger Carmel Formation unconformably rest upon the Lower Jurassic Navajo Sandstone, with the contact correlated to the regionally extensive J-1 Unconformity (Pipiringos & O'Sullivan, 1978; Kocurek & Hunter, 1986). The unconformity is characterised by an undulating palaeotopography that is inherited from differential erosion of the underlying Navajo Sandstone generated by a widespread regional uplift event (Marzolf, 1991; Bromley, 1992). Where preserved, isolated occurrences of sediments of the Temple Cap Formation across the margin represent the early aeolian developmental stage of the system. They are capped by a composite regressive surface (CR1) onto which the transgressive tract of the lower marine tongue of the Judd Hollow Member of the Carmel Formation is deposited. The

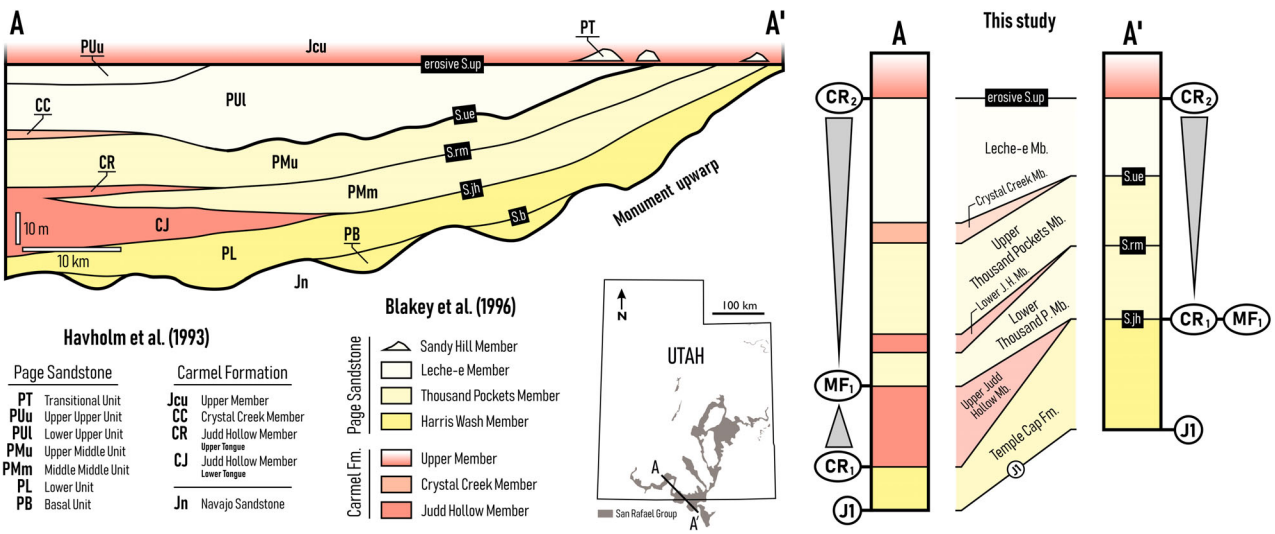

Fig. 2. Schematic framework of the Temple Cap and Page Sandstone, illustrating sequence stratigraphical surfaces and nomenclature used in this study. The figure correlates the stratigraphical sub-divisions used in this study to those of previous work in Havholm *et al.* (1993) and Blakey *et al.* (1996).

© 2026 The Author(s). *Sedimentology* published by John Wiley & Sons Ltd on behalf of International Association of Sedimentologists, *Sedimentology*, **73**, 2081–2119

13653091, 2026, 6, Downloaded from https://onlinelibrary.wiley.com/doi/10.1111/sed.70126 by British Geological Survey, Wiley Online Library on [15/10/2026]. See the Terms and Conditions (https://onlinelibrary.wiley.com/terms-and-conditions) on Wiley Online Library for rules of use; OA articles are governed by the applicable Creative Commons License

maximum flooding surface (MF1) and its associated condensed horizons (see Facies Association 11 in Hême de Lacotte *et al.*, 2026) mark the top of this system tract. The inland expression of this transgressive system tract is characterised by a condensed regional super surface corresponding to both CR1 and MF1 ('S-jh', *sensu* Havholm *et al.*, 1993; Fig. 2).

Sediments of the aeolian Thousand Pockets Member of the Page Sandstone correspond to the initiation of the following regressive system tract and may be subdivided into lower and upper units by a second thin package of the Judd Hollow Member ('S-rm', *sensu* Havholm *et al.*, 1993). The top of the Thousand Pockets Member is marked by the occurrence of an erosive and irregular deflationary super surface ('S-ue', *sensu* Havholm *et al.*, 1993) that is interpreted as the inland expression of processes occurring contemporaneously with the deposition of the supratidal-dominated Crystal Creek Member. Sediments of the following aeolian Leche-e Member correspond to the further development of the regressive system tract and the final stage of this first T–R sequence. The member is capped by a gradually erosive composite regressive surface (CR2) that increasingly truncates the Page Sandstone southeast of Page ('S-up' *sensu* Havholm *et al.*, 1993). Mixed fluvial to supratidal sediments of the second T–R sequence of the Carmel Formation are deposited unconformably upon the CR2 surface (Bowler, 2026). Jurassic strata have been entirely eroded in western Utah and Nevada due to the eastward propagation of the Cretaceous Sevier thrust front and the generation of a widespread bevelled unconformity (cf. Buckhorn Conglomerate at the base of the Cedar Mountain Formation; Currie, 1997; Roca & Nadon, 2007).

Studies on the Page Sandstone have led to the development of key founding principles in aeolian sedimentology (i.e. Havholm *et al.*, 1993; Havholm & Kocurek, 1994; Kocurek *et al.*, 2001) and strengthened early models for the response of aeolian systems to cyclically fluctuating water table levels, something that is now well constrained (e.g. Mountney, 2012 and references therein). Renewed interest in the sediments of the Page Sandstone has highlighted the complexity of outcrop-scale architectural complexity of such systems caused by strong autogenic masking phenomena (Cardenas *et al.*, 2019). Its exceptional exposure across extensive areas enables investigation of these observations in a broader context and their linkage to overarching allogenic controls.

METHODOLOGY

Twenty-six sedimentary logs have been collected across the regionally extensive outcrop belt of the marine to coastal Carmel Formation and the aeolian Temple Cap Formation and Page Sandstone in southern Utah and northern Arizona. Two NW–SE transects of 84 km and 53 km, composed of four and three sections, respectively, constitute the basis for palaeoshoreline-perpendicular correlation panels across the intertonguing zone between the two depositional realms (Fig. 3). The framework presented in this study works towards combining recent chronological findings (cf. Dickinson *et al.*, 2010) with the current lithostratigraphical framework by treating contemporaneous mappable units as one package that contains internally differing depositional environments. Details of the correspondence between the sequence-stratigraphical framework used in this study and the informal units from Havholm *et al.* (1993) and Blakey *et al.* (1996) are shown in Fig. 2, which can be considered as a simplified version of the correlation panel A presented later in this work (Fig. 8A). The regional composite regressive surface CR2, associated with the termination of the aeolian Page Sandstone, and in places with its partial erosion, provides a physical stratigraphical marker for correlation between sections. This surface has been attributed previously to the top sequence boundary of the first T–R sequence represented by the deposits of the Carmel Formation (Hême de

Fig. 3. Outcrop distribution map of the San Rafael Group and contemporaneous Middle Jurassic strata (Hintze *et al.*, 2000) with locations of studied sections and outcrop panels. This study focuses on two shoreline-perpendicular correlation panels between sections 9 to 15 (Fig. 8A) and sections 6 to 8 (Fig. 8B). The position of the transect discussed in Hême de Lacotte *et al.* (2026) is also given for context. Elevation data derived from open access digital elevation models accessible via the USGS EarthExplorer platform (https://earthexplorer.usgs.gov).

© 2026 The Author(s). *Sedimentology* published by John Wiley & Sons Ltd on behalf of International Association of Sedimentologists, *Sedimentology*, **73**, 2081–2119

13653091, 2026, 6, Downloaded from https://onlinelibrary.wiley.com/doi/10.1111/sed.70126 by British Geological Survey, Wiley Online Library on [15/10/2026]. See the Terms and Conditions (https://onlinelibrary.wiley.com/terms-and-conditions) on Wiley Online Library for rules of use; OA articles are governed by the applicable Creative Commons License

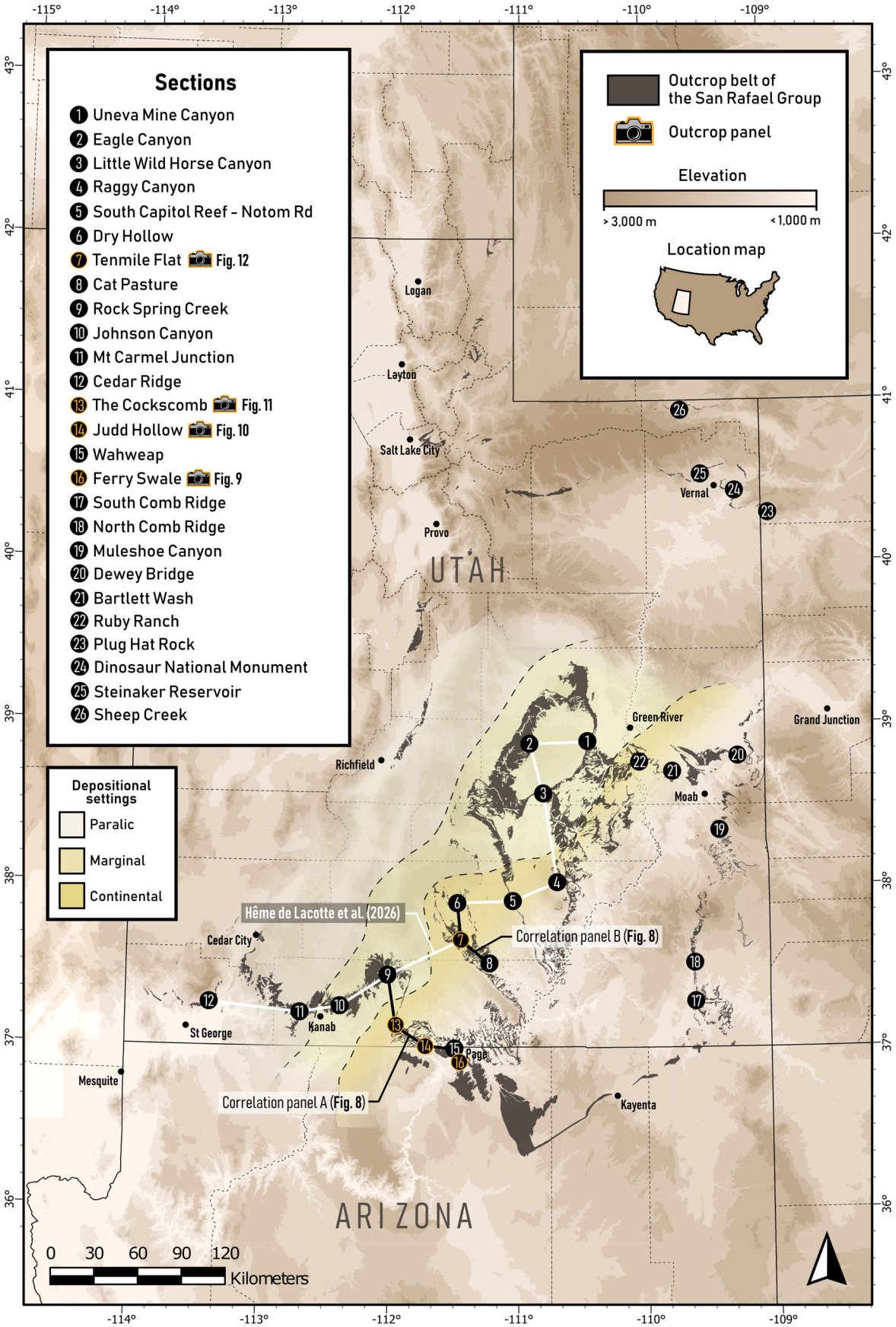

13653091, 2026, 6, Downloaded from https://onlinelibrary.wiley.com/doi/10.1111/sed.70126 by British Geological Survey, Wiley Online Library on [15/10/2026]. See the Terms and Conditions (https://onlinelibrary.wiley.com/terms-and-conditions) on Wiley Online Library for rules of use; OA articles are governed by the applicable Creative Commons License

Lacotte *et al.*, 2026). Interpreted transgressive and regressive system tracts are bounded by maximum flooding surfaces (MF) and composite regressive surfaces (CR). The latter are constituted of, from distal to proximal settings, true marine maximum regressive surfaces, diastemic transgressive ravinement surfaces and inland deflationary super surfaces equivalent to subaerial unconformities in Embry (2010)'s model.

Recognition of key genetic aeolian sequence boundaries is based upon the investigation of outcrop-scale super surfaces (i.e. 'Stokes surfaces', Stokes, 1968; Loope, 1985; Kocurek, 1988), coupled with the observation of bed-scale diagnostic features indicative of long-lasting aeolian deflation events to water table levels. Outcrop-scale deflationary super surfaces are recorded by regionally correlative sharp truncation surfaces of planar to undulatory geometries (e.g. Gross *et al.*, 2023) overlain by dune cross-stratification sets of the following sequence. They differ from basal bounding surfaces of scour-and-fill complexes by their homogenous and low-relief erosive character. Bed-scale indicators of deflationary super surfaces include evidence of pedogenesis such as rhyzoliths-rich horizons (Langford & Chan, 1988) or large-scale polygonal fracture patterns linked to the development of surficial evaporitic crusts from groundwater salt precipitation (Kocurek & Hunter, 1986).

Detailed analysis of sedimentological, architectural, ichnological, paleontological and palaeocurrent data has led to the identification of twenty facies (Table 1) that are grouped into eight architectural elements. Relative architectural element proportions have been calculated for the sections presented in this study. Facies distribution maps were constructed for three time surfaces (CR1, MF1 and MF2) by extrapolating observed contemporaneous facies between each logged section. Approximate positions and the extents of topographical palaeohighs were compiled from the literature (Blakey *et al.*, 1983, 1988; Peterson, 1988; Havholm *et al.*, 1993; Bjerrum & Dorsey, 1995; Kowallis *et al.*, 2001), along with the extent of the Sevier thrust front responsible for Cretaceous regional stratal erosion (Doelling *et al.*, 2013; Sprinkel *et al.*, 2024).

Photogrammetric panels at four locations (Sections 7, 13, 14 and 16; Fig. 3) have been compiled into three-dimensional digital outcrop models to characterise changes in sedimentary architectures and geometrical relationships across the erg margin. Interpreted architectural elements have been mapped onto orthomosaic images derived from digital outcrop models. Orthomosaic plan projections were manually oriented normal to local structural dips, and parallel to outcrops plans, to display true architectural element geometries. Key sequence stratigraphical surfaces have been annotated onto each orthomosaic and correspond to system tracts boundaries of the Carmel Formation. When evident, internal super surfaces observed by Havholm *et al.* (1993) have been marked.

SEDIMENTARY FACIES AND ARCHITECTURAL ELEMENTS

Twenty lithofacies resulting from a mixture of aeolian, tidal, wave action and evaporitic processes have been recognised in this study within the sediments of the Temple Cap Formation, Carmel Formation and Page Sandstone (Figs 4 to 6; Table 1). These facies are grouped into eight architectural elements consisting of predictable geometrical arrangements of facies in two-dimensional cross-sections (Fig. 7). These architectural elements are deposited in two overarching depositional systems, including aeolian and shallow-marine settings.

Aeolian architectural elements

Climbing aeolian dune element (A1)

Description. Elements of this type are characterised by extensive tabular bodies bounded by outcrop-scale super surfaces (*sensu* Kocurek, 1988; Fig. 7). They range from 100 to 1000 m in length and from 5 to 20 m in thickness and are observed everywhere across the study area. Climbing dune elements (A1) dominantly comprise metre-thick sets of planar (Axs) to trough cross-stratified (Atxs) aeolian sandstones. A1 elements may be sporadically interbedded with lenses of aeolian interdune sediments (A2). Cross-stratification sets present alternating couplets of reverse-graded coarser deposits draped by finer material, which occasionally grade into horizontal laminations (Ap) at the base of set boundaries (Fig. 4B). Sharp contacts with underlying crinkly laminated sandstones (Acr) are sporadically observed (Fig. 4A and C). Straight cross-stratification sets (Axs) are usually observed at the base of this element and present a gradual vertical transition into trough cross-stratification sets (Atxs), which is expressed as

© 2026 The Author(s). *Sedimentology* published by John Wiley & Sons Ltd on behalf of International Association of Sedimentologists, *Sedimentology*, **73**, 2081–2119

13653091, 2026, 6, Downloaded from https://onlinelibrary.wiley.com/doi/10.1111/sed.70126 by British Geological Survey, Wiley Online Library on [15/10/2026]. See the Terms and Conditions (https://onlinelibrary.wiley.com/terms-and-conditions) on Wiley Online Library for rules of use; OA articles are governed by the applicable Creative Commons License

Table 1. Summary of lithofacies observed in the aeolian to marine Temple Cap Formation, Carmel Formation and Page Sandstone system.

Code	Facies	Architectural element(s)	Texture	Structures	Processes
Axs	Straight cross-stratified aeolian sandstone	A1	Grey to yellow, fine to coarse-grained, well sorted, well-rounded, clast-supported quartz grains	Tabular cross-stratification sets with bimodal grain-size foreset couplets truncated by reactivation surfaces	Episodic gravity-driven avalanching events on the lee-slope of straight-crested migrating aeolian bedforms (i.e. grain flow) during continuous settlement of suspended load (i.e. grain fall)
Atxs	Trough cross-stratified aeolian sandstone	A1	Grey to yellow, fine to coarse-grained, well sorted, well-rounded, clast-supported quartz grains	Trough cross-stratification sets with bimodal grain-size foreset couplets truncated by reactivation surfaces	Episodic gravity-driven avalanching events on sinuous-crested migrating aeolian bedform lee-slope (i.e. grain flow) during continuous settlement of suspended load (i.e. grain fall)
Asc	Scour-infill cross-stratified aeolian sandstone	A4	Grey to yellow, fine to coarse-grained, well sorted, well-rounded, clast-supported quartz grains	Amalgamated coset of multi-directional cross-stratification sets with irregular erosive bases and bimodal grain-size foreset couplets truncated by reactivation surfaces	Localised scouring due to aerodynamic turbulences, filled by episodic gravity-driven avalanching events on barchanoid aeolian bedform lee-slope (i.e. grain flow) during continuous settlement of suspended load (i.e. grain fall)
Acl	Climbing cross-stratified aeolian sandstone	A4	Grey to yellow, fine to coarse-grained, well sorted, well-rounded, clast-supported quartz grains	Low-angle cross-stratification sets with occasional critically to super-critically climbing cross-stratification sets and rare topsets and stoss-slope preservation	Aggrading windblown sediment on dry and unstabilised interdune hollows with exceptional preservation of aeolian protodune migration and gradual lee-slope development
Asup	Superimposed cross-bedding	A3	Grey to yellow, fine to coarse-grained, well sorted, well-rounded, clast-supported quartz grains	Superimposed downlapping cross-stratification sets with bimodal grain-size foreset couplets truncated by reactivation surfaces. Negative bedform angle of climb	Gravity-driven avalanching events on the lee-slope of superimposed aeolian bedform trains constituting the leeward face of a draa
Acr	Crinkly laminated	A2	Yellow to rusty orange, very fine to medium-grained, well	Isolated crinkly to undulating planar lamination sets with	Suspended load trapping on dampened

13653091, 2026, 6, Downloaded from https://onlinelibrary.wiley.com/doi/10.1111/sed.70126 by British Geological Survey, Wiley Online Library on [15/10/2026]. See the Terms and Conditions (https://onlinelibrary.wiley.com/terms-and-conditions) on Wiley Online Library for rules of use; OA articles are governed by the applicable Creative Commons License

Table 1. (continued)

Code	Facies	Architectural element(s)	Texture	Structures	Processes
	aeolian sandstone		sorted, well-rounded, clasts supported quartz grains	adhesion structures and vertically aggrading wavy cryptalgal mat laminations	to wet interdune surface
Ap	Horizontally laminated aeolian sandstone	A2, A4	Grey to yellow, medium to coarse-grained, moderately to well sorted, sub-rounded, clast-supported quartz grains	Impact ripple and pinstripe lamination sets	Suspended load settlement and migrating impact ripples on aeolian dune plinth
Ab	Brecciated aeolian sandstone	M1	*Clasts*: pebble- to boulder size lithified intraclasts of *Asx* and *Atxs* facies. *Matrix*: Grey to yellow, medium to coarse-grained, well to moderately sorted, well-rounded, clasts supported quartz grains	Laterally continuous to trough cross-stratification sets with contorted bimodal grain-size foreset couplets. Truncated topsets with irregular, highly cemented and laterally extensive top bounding surfaces. Metre-scale polygonal fractures with intense soft-sediment deformation, occasional rhizoliths, burrows and chert concretion	Dampened and fracturing of pre-lithified aeolian deposits by secondary evaporitic crust surface generation related to salt precipitation in groundwater capillary fringe
Aco	Contorted aeolian sandstone	M2	Yellow to pale red, fine to medium-grained, moderately sorted, well-rounded, clast-supported quartz grains	Structureless sandstones with bleached and contorted strata. Occasional water escape structures, microfaulting and oxidised indurated top surfaces	Contorted water-saturated aeolian sediment with intense burial-induced deformation
Mxs	Cross-stratified to structureless sandstone	M1	Grey to yellow, very fine to medium-grained, poorly to well sorted, sub- to well rounded, clast-supported quartz grains	Laterally continuous structureless sandstones occasionally displaying decimetre-scale cross-stratification sets with intense soft-sediment deformation	Subaqueous reworking of aeolian sediment under unidirectional non-Newtonian fluid flow, occasionally preserving subaqueous bedforms and plane beds formed under waning subcritical flows
Mwr	Oscillatory rippled sandstone	M1	Grey to yellow, very fine to medium-grained, poorly to well sorted, sub- to well rounded, clast-supported quartz grains	Tabular ripple cross-lamination sets displaying well-developed current to oscillation ripple forms. Peak-crested oscillation ripple forms may be observed in cross-section views	Subaqueous reworking of aeolian sediment under oscillatory currents

13653091, 2026, 6, Downloaded from https://onlinelibrary.wiley.com/doi/10.1111/sed.70126 by British Geological Survey, Wiley Online Library on [15/10/2026]. See the Terms and Conditions (https://onlinelibrary.wiley.com/terms-and-conditions) on Wiley Online Library for rules of use; OA articles are governed by the applicable Creative Commons License

Table 1. (continued)

Code	Facies	Architectural element(s)	Texture	Structures	Processes
Mmi	Microbial dolomicrite	M2	Light yellow to reddish, interbedded silts to very fine quartz grains and dolomicrite	Columnar stromatoliths to stratiform cryptalgal dolomicrite lamination sets with smooth to peak-crested oscillation ripple cross-lamination sets	Microbially induced carbonate precipitation coupled with the trapping of terrigenous material in very shallow water depths
Mgy	Crystalline evaporite	M2	White to pale green, chicken-wire gypsum and folded anhydrite beds	Laminated to massive laterally discontinuous and highly contorted units	Salt precipitation on evaporitic sabkha playa
Mred	Poorly stratified red silt- to mudstone	M2	Reddish to dark brown, moderately sorted silts and clay	Laterally extensive, poorly stratified siltstone and mudstone. Decimetre-scale desiccation cracks displaying fan-like sub-vertical stratifications recording progressive filling with *Asx* and *Atsx* material	Silt and clay material deposited under very low to null subaqueous bed shear-stress conditions
Mht	Heterolithic ripple cross-laminated sandstone	M3	Light yellow, very fine to fine-grained, well to moderately sorted, well to sub-rounded, clasts supported quartz grains	Sand dominated heterolithic stratifications with bifurcating to ladderback oscillation ripple forms exposed in plan view. Occasional moderate ichnological index (*Cruziana* ichnofacies) and nodular gypsum. Interbedded with clay drapes	Subaqueous grains entrainment by oscillatory currents and clay settlement under occasional null subaqueous bed shear-stress conditions
Mma	Plane-bedded marls	M3	Pale blue grey mudstone (50%) and light green clay (50%)	Thick and extensive plane-bedded units	Mixed terrigenous clay and carbonate mud particles settlement in null bed shear-stress conditions
Mhcs	Hummocky cross-stratified sandstone	M4	Light yellow very fine to fine-grained, moderately to well sorted, sub-rounded, clast-supported quartz grains	Hummocky and swaley cross-stratification sets	Subaqueous grains entrainment by the superimposition of mutlidirectional currents
Mlxs	Low-angle cross-stratified sandstone	M4	Light yellow very fine-grained, well-sorted, clast-supported quartz grains	Extensive low-angle cross-stratification sets with occasional upper-flow regime parallel lamination sets and rare oscillatory ripple cross-lamination sets. Often associated with *Mhcs*	High-energy and multi-directional subaqueous sediment remobilisation

© 2026 The Author(s). *Sedimentology* published by John Wiley & Sons Ltd on behalf of International Association of Sedimentologists, *Sedimentology*, **73**, 2081–2119

13653091, 2026, 6, Downloaded from https://onlinelibrary.wiley.com/doi/10.1111/sed.70126 by British Geological Survey, Wiley Online Library on [15/10/2026]. See the Terms and Conditions (https://onlinelibrary.wiley.com/terms-and-conditions) on Wiley Online Library for rules of use; OA articles are governed by the applicable Creative Commons License

Table 1. (continued)

Code	Facies	Architectural element(s)	Texture	Structures	Processes
Moxs	Cross-stratified oolitic grainstone	M4	Light grey oolitic and bioclastic wackestone to grainstone	Extensive cross-stratified wackestone to grainstone with occasional reactivation surfaces, bidirectional foresets azimuths and lenses of accumulated bioclastic debris. Presence of mud drapes at cross bedding toesets	Subaqueous dune migration under bidirectional subcritical flow with unsteady bed shear-stress conditions
Mca	Bioclastic wackestone	M4	Light grey bioclastic wackestone	Thick plane-bedded and laminated wackestone with occasional vertical burrows and trace fossils	Subaqueous carbonate particles settling in calm conditions, occasionally disrupted by bioclastic deposition during rare events of higher energy

an increasing variance in the dip directions of foresets.

Interpretation. Elements of this type are interpreted as the preservation of simple transverse aeolian dune migration and climb under relatively low water table conditions. In this scenario, bedform migration is the result of grainflow avalanching events combined with continuous grainfall settlement of suspended load (Hunter, 1977; Kocurek & Dott, 1981). Contrasting geometries between straight (Axs) and trough cross-stratified (Atx) sets can be linked to differences in dune crest-line sinuosities (Rubin & Hunter, 1982). Vertical transitions from straight-crested to sinuous-crested aeolian dunes indicate increased bedform interactions in maturing dune fields (Ewing & Kocurek, 2010; Kocurek *et al.*, 2010). The occurrence of interdune elements (A2) interbedded with A1 is attributed to the co-migration of aeolian bedforms and interdune corridors during occasional periods of elevated water table (Kocurek, 1981; Crabaugh & Kocurek, 1993). Overall, climbing aeolian dune elements are associated with sediment availability conditions commonly linked to early-stage development of a dune field (i.e. aeolian construction, *sensu* Mountney, 2006) and/or marginal physiographic location (Mountney & Thompson, 2002).

Aeolian interdune element (A2)

Description. Elements of this type are characterised by isolated metre-scale lenticular bodies (Fig. 7) but may sporadically be observed as laterally extensive kilometre-scale sheets. They

Fig. 4. Examples of aeolian lithofacies observed in the Temple Cap Formation and Page Sandstone. (A) Tabular aeolian dune cross-stratification set (Axs) migrating over a wet interdune surface composed of fine-grained crinkly laminated sandstone (Acr). Note the development of rhyzoliths at the contact between the two facies suggesting static water table conditions over a significant amount of time. (B) Interfingering relationships between grainflow deposits (Axs) and wind-ripple strata (Ap) at the toesets of an aeolian dune. (C) Localised undulating microbial mat laminations recorded within crinkly laminated sandstone (Acr) suggesting periods of standing water within interdune corridors. (D) Pinstripe laminations (Ap) recording the aggradation of a dry interdune floor through the migration of windblown impact ripples. (E) Scoured blowout surface (Sc) followed by secondary filling of an aeolian dune (Asc). (F) Exceptional preservation of downward climbing cross-stratified set (Acl) associated to the migration of an incipient aeolian dune. Note preserved stoss-slope laminations and subsequent bedform crest-line knickpoints (white arrows) migrating towards the right side of the photomosaic.

© 2026 The Author(s). *Sedimentology* published by John Wiley & Sons Ltd on behalf of International Association of Sedimentologists, *Sedimentology*, **73**, 2081–2119

13653091, 2026, 6, Downloaded from https://onlinelibrary.wiley.com/doi/10.1111/sed.70126 by British Geological Survey, Wiley Online Library on [15/10/2026]. See the Terms and Conditions (https://onlinelibrary.wiley.com/terms-and-conditions) on Wiley Online Library for rules of use; OA articles are governed by the applicable Creative Commons License

Lithofacies observed in aeolian architectural elements

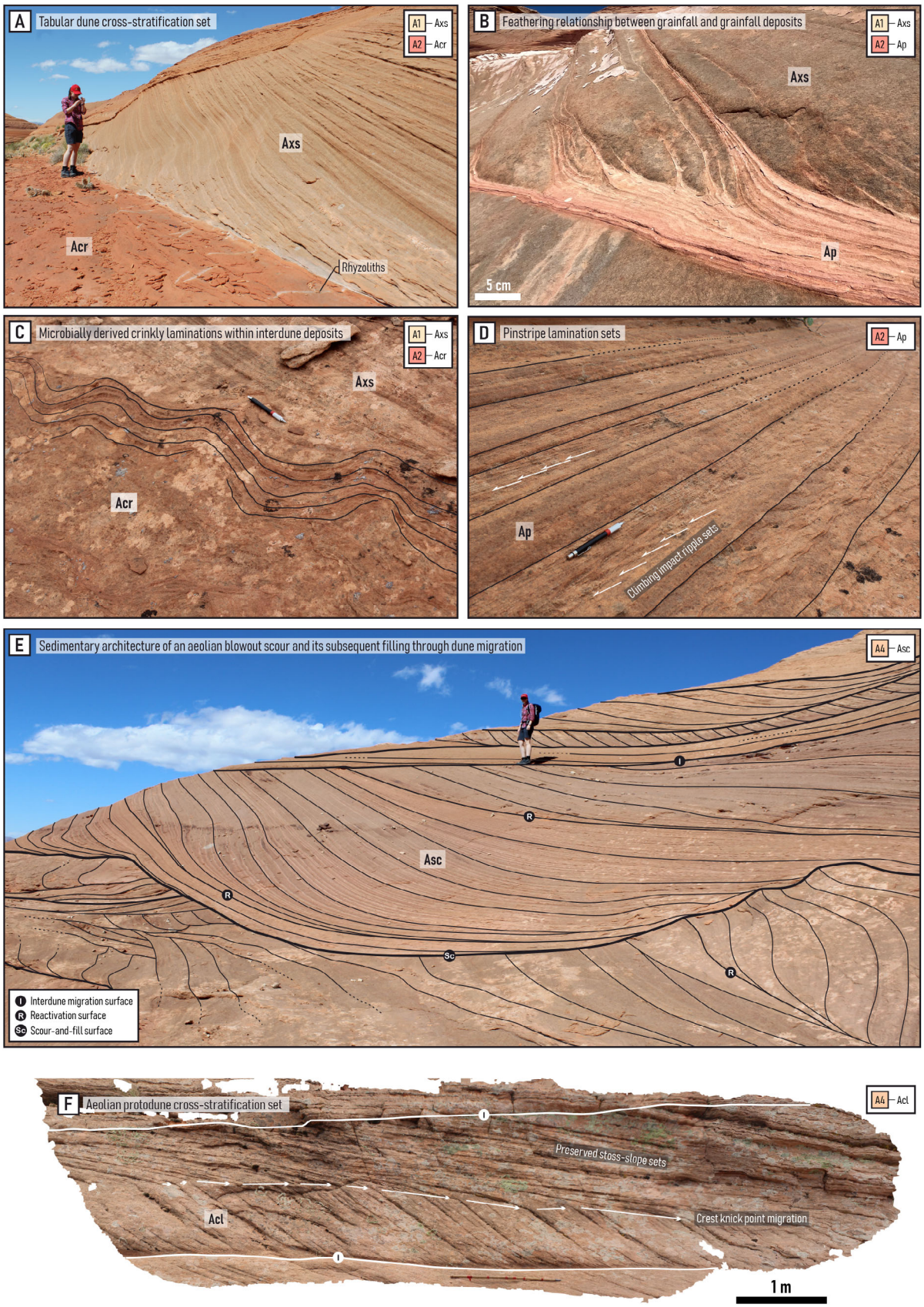

© 2026 The Author(s). *Sedimentology* published by John Wiley & Sons Ltd on behalf of International Association of Sedimentologists, *Sedimentology*, **73**, 2081–2119

13653091, 2026, 6, Downloaded from https://onlinelibrary.wiley.com/doi/10.1111/sed.70126 by British Geological Survey, Wiley Online Library on [15/10/2026]. See the Terms and Conditions (https://onlinelibrary.wiley.com/terms-and-conditions) on Wiley Online Library for rules of use; OA articles are governed by the applicable Creative Commons License

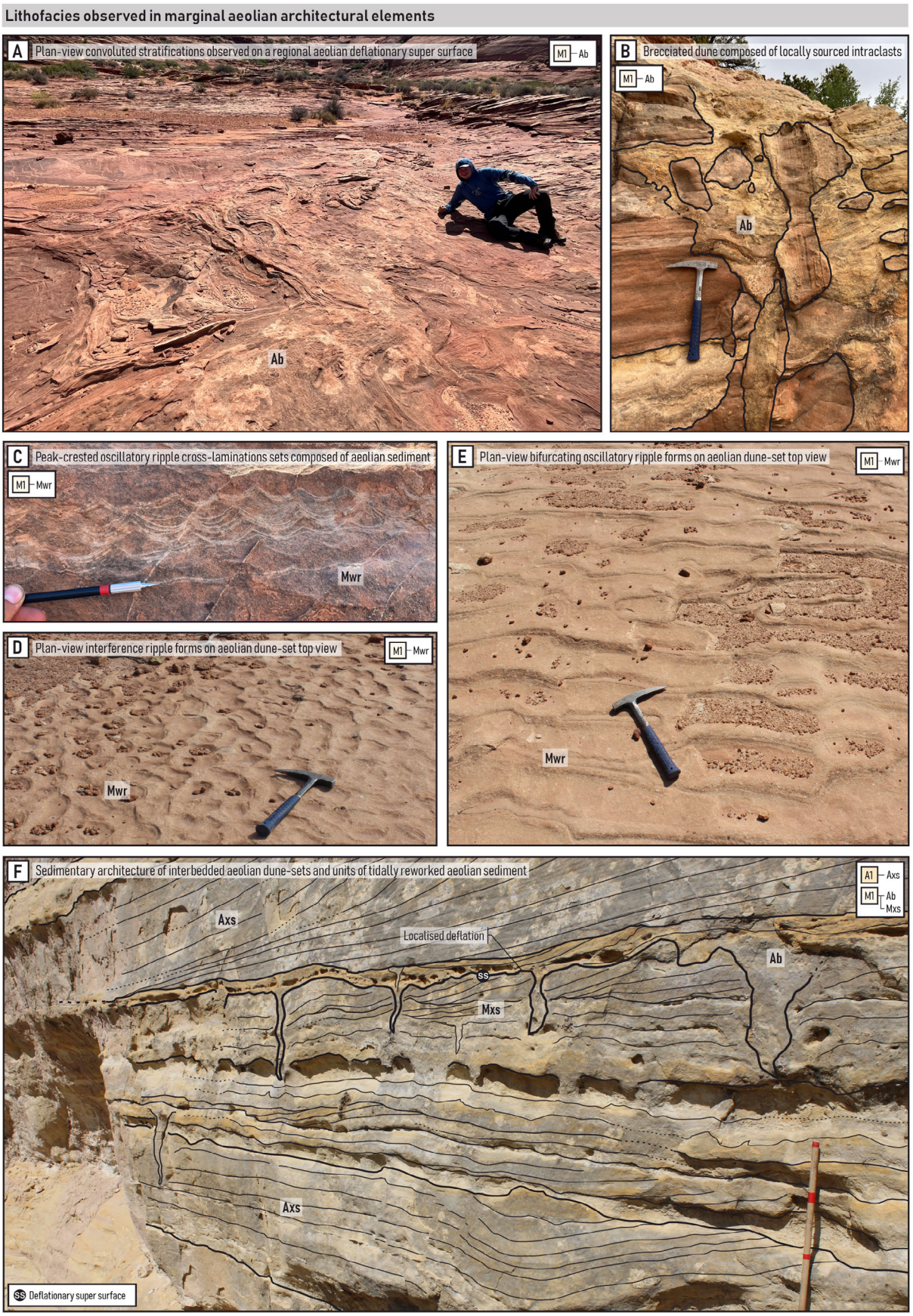

13653091, 2026, 6, Downloaded from https://onlinelibrary.wiley.com/doi/10.1111/sed.70126 by British Geological Survey, Wiley Online Library on [15/10/2026]. See the Terms and Conditions (https://onlinelibrary.wiley.com/terms-and-conditions) on Wiley Online Library for rules of use; OA articles are governed by the applicable Creative Commons License

Fig. 5. Examples of marginal aeolian lithofacies observed in the Temple Cap Formation, Carmel Formation and Page Sandstone. (A) Plan-view perspective of deformed and brecciated aeolian cross-stratified sets (Ab) associated with a regionally extensive deflationary super surface (J-1 Uncomformity). (B) Cross-section view of lithified aeolian dune intraclasts within a large polygonal fracture fill (Ab) associated with long-term deflation to the water table level. (C–E) Cross-section and plan views of oscillatory ripple laminated aeolian sandstone (Mwr). (F) Interbedded sets of small aeolian dune cross-stratification sets (Axs) and tidally reworked aeolian material (Mxs). Note the presence of brecciated aeolian sandstone (Ab) betraying the expression of a partial deflation.

comprise crinkly (Acr) and horizontally laminated (Ap) aeolian sandstones that grade from one facies to another. Crinkly laminated (Acr) sandstone beds may display rhyzoliths on their top surface (Fig. 4A) and undulating internal fabrics (Fig. 4C). Horizontally laminated (Ap) sandstone beds occasionally display pinstripe cross-lamination sets (Fig. 4D). Aeolian interdune elements are typically interbedded within sets of climbing aeolian dune elements (A1; Fig. 12A). Basal contacts with underlying aeolian dune elements are usually flat and erosive, while upper contacts can sporadically display transitional upper contacts (i.e. 'feathering'), with overlying aeolian dune cross-stratification toesets (Axs/Atxs; Fig. 4A and B).

Interpretation. Lenticular elements of this type are interpreted as the record of aggrading sediments in restricted interdune corridors deposited under variable water table dynamics while their laterally extensive analogues are more probably associated to deflationary stages and aggrading continental sabkhas. Very fine-grained windblown material is interpreted to have been preferentially preserved through trapping processes controlled by surface dampness conditions at the time of deposition. Crinkly lamination sets (Acr) are interpreted to be the preserved product of adhesion structures (Kocurek & Fielder, 1982), which are formed onto dampened interdune surfaces where microbial communities may sporadically develop (McKay *et al.*, 2016). Rhyzoliths are indicative of static water table conditions at the sediment surface (Loope, 1988; Cosgrove *et al.*, 2022). Dry interdune surfaces allowed the migration of impact ripples and their preservation as horizontally laminated sandstones (Ap; Hunter, 1977). The differences in relationship between dune cross-stratified toesets and underlying laminations reflect variable water table dynamics during the migration of aeolian bedforms (Mountney & Thompson, 2002).

Compound transverse draa element (A3)

Description. Elements of this type are characterised by large and regionally extensive units (Fig. 7) concentrated in the continental-most parts of the study area (Fig. 3). They range from 100 to 1000 m in length and from 10 to 50 m in thickness. They are almost exclusively composed of cosets of superimposed cross-stratified aeolian sandstone beds (Asup) that differ from other aeolian facies by the internal downlapping architectures of their cross-stratified sets and associated set bounding surfaces (Fig. 9). Sporadic occurrences of horizontally laminated sandstones (Ap) are observed. Coset-bounding surfaces are usually observed as oblique and erosive contacts (Fig. 9).

Interpretation. Elements of this type are interpreted as the record of migrating large compound draa bedforms composed of superimposed transverse dunes (Asup; Brookfield, 1977; Rubin & Hunter, 1983; Mountney *et al.*, 1999). Their generation is associated with very mature developmental stages of the dune field, where large compound bedforms evolved from simple dune trains (e.g. Mountney & Howell, 2000; Kocurek & Day, 2018; Abrantes Jr *et al.*, 2020; Mesquita *et al.*, 2021). Cross-cutting coset-bounding surfaces are interpreted as draa migration surfaces (Mountney, 2006) and were generated by the migration and partial erosion of succeeding draas. Sporadic preservation of horizontal laminations (Ap) is attributed to the migration of impact ripples at the plinths of superimposed dunes.

Amalgamated aeolian scour-and-fill complex (A4)

Description. Elements of this type are characterised by metre-thick, erosive, lensoidal bodies concentrated along coset-bounding surfaces of compound transverse draa elements (A3) and are largely observed in the continental-most parts of the system (Figs 3 and 7). Scour-filling

© 2026 The Author(s). *Sedimentology* published by John Wiley & Sons Ltd on behalf of International Association of Sedimentologists, *Sedimentology*, **73**, 2081–2119

13653091, 2026, 6, Downloaded from https://onlinelibrary.wiley.com/doi/10.1111/sed.70126 by British Geological Survey, Wiley Online Library on [15/10/2026]. See the Terms and Conditions (https://onlinelibrary.wiley.com/terms-and-conditions) on Wiley Online Library for rules of use; OA articles are governed by the applicable Creative Commons License

Lithofacies observed in tidal architectural elements

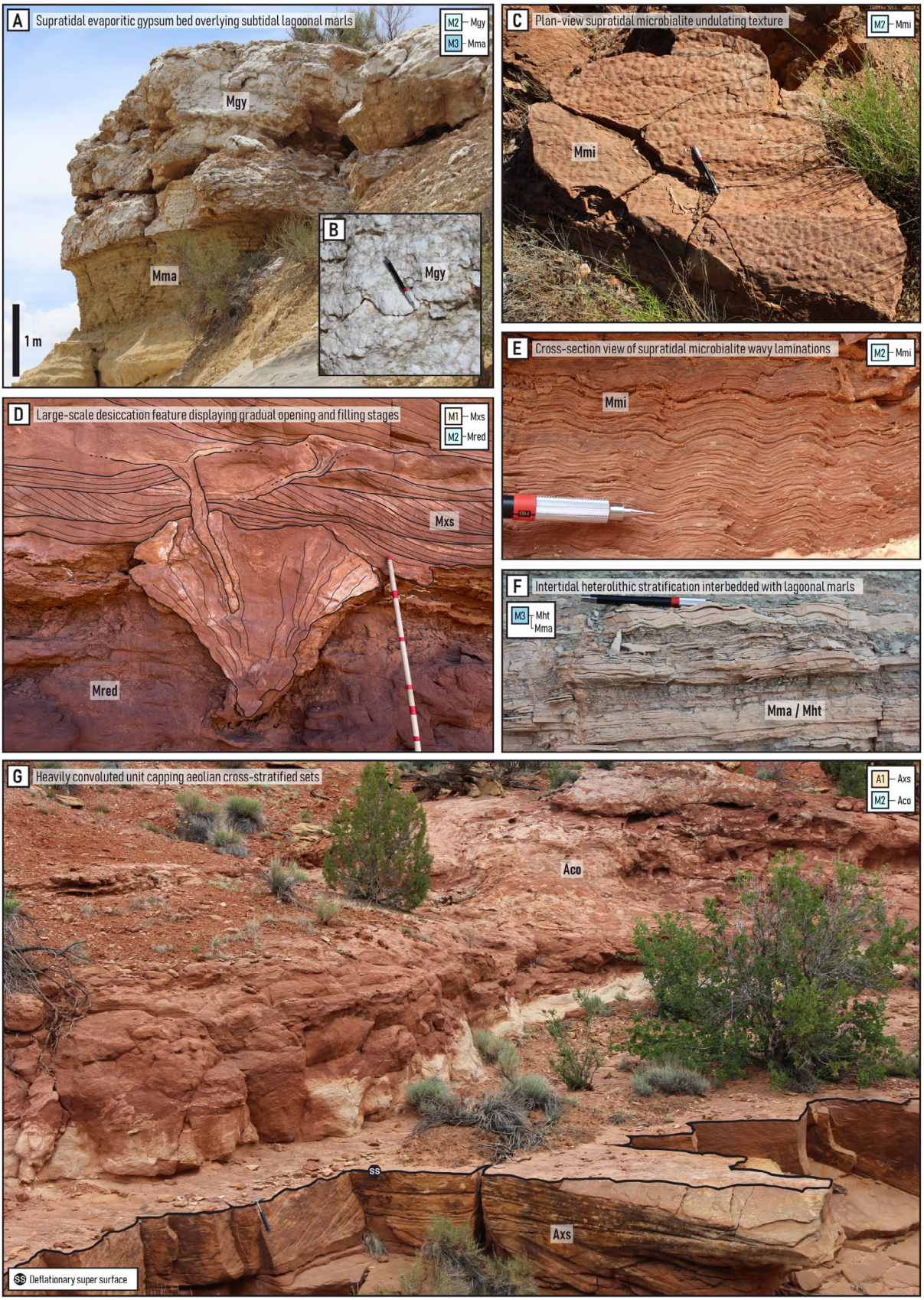

13653091, 2026, 6, Downloaded from https://onlinelibrary.wiley.com/doi/10.1111/sed.70126 by British Geological Survey, Wiley Online Library on [15/10/2026]. See the Terms and Conditions (https://onlinelibrary.wiley.com/terms-and-conditions) on Wiley Online Library for rules of use; OA articles are governed by the applicable Creative Commons License

Fig. 6. Examples of supratidal and intertidal lithofacies observed in the Carmel Formation. (A, B) Thick evaporitic bed composed of recrystallised anhydrite (Mgy) capping lagoonal marls deposits (Mma). (C) Plan-view of supratidal microbial mat surface (Mmi) displaying undulating textures. (D) Deep and wide desiccation feature occurring within terrigenous clay (Mred) revealing gradual opening and filling with sandy material from overlying subaqueous dune cross-stratified sets (Mxs). (E) Cross-section view of supratidal microbial mat (Mmi). (F) Intertidal heterolithic stratification (Mht) interbedded with lagoonal marl deposits (Mma). Note sporadic preservation of peak-crested oscillatory ripple cross-laminations. (G) Heavily contorted aeolian dune unit (Aco) capping aeolian cross-stratified sets (Axs). Note the sharp truncation surface interpreted as a deflationary super surface (SS).

cross-stratified aeolian sandstones (Asc; Fig. 4E) comprise most of this element. Isolated scour-filled lenses range typically from 5 to 20 m wide although they can define amalgamated sheet-like complexes (i.e. belts) of multiple cross-stratification sets cross-cutting each other (Fig. 9). Exceptional preservation of downward climbing cross-stratified aeolian sandstones (Acl) may occur in wind transport-parallel sections and commonly grade laterally from low-angle stratifications and horizontal laminations sets (Ap; Fig. 4F).

Interpretation. Elements of this type are interpreted as amalgamated scour-and-fill complexes generated by bedform cannibalisation triggered by localised autogenic mechanisms (Cardenas *et al.*, 2019). In such scenarios, local scour-filling cross-stratified sets (Asc) record the migration of dunes into topographical lows previously eroded as wind blowouts (e.g. Kocurek & Day, 2018; Ferronatto *et al.*, 2019; Roberts *et al.*, 2025). It is unlikely that this type of element was formed by channelised subaqueous processes, largely as preserved thicknesses of scour-filling cross-stratification sets and scoured depths are inconsistent with geometric parameters of fluvial channels occurring in arid environments (cf. Gibling, 2006; Priddy & Clarke, 2020). Lateral transitions from horizontal laminations (Ap) to downward climbing cross-stratified sets (Acl) are interpreted to record the initiation stage of aeolian bedform development within the topographical lows of blowout scours or within the troughs of larger dunes (Phillips *et al.*, 2019). When preserved as extensive sheet-like complexes, these elements are interpreted as the sedimentary products of autogenic aeolian processes linked to mature dune fields undergoing negligible aggradation (Cardenas *et al.*, 2019).

Shallow-marine architectural elements

Tidally reworked aeolian dune element (M1)

Description. Elements of this type are characterised by extensive tabular units, displaying numerous lithofacies, linked to variable processes, that were deposited in a composite system of competing environments (Fig. 7). They are commonly intercalated with climbing aeolian dune elements (A1) and supratidal flat elements (M2; Fig. 12B). They range from 100 to 1000 m in length and from 1 to 10 m in thickness and are mainly observed in marginal parts of the study area (Fig. 3). They are composed of cross-stratified to structureless subaqueous sandstone beds (Mxs), which are interbedded with oscillatory rippled (Mwr) and brecciated (Ab) sandstone beds. Subaqueous strata (Mxs) are composed of well rounded and sorted material reworked from aeolian units and are generally defined by decimetre-thick sets with irregular and generally erosive basal set bounding surfaces (Fig. 5F). When visible, cross-stratification geometries are crude and present irregular lamination surfaces, with occasional convolute laminations. Cross-stratification sets are commonly interbedded with plane beds of similar lithological composition. Oscillatory ripple laminated sandstone beds (Mwr) are typically composed of sediment originating from aeolian cross-stratified sandstone (Axs; Fig. 5C). When observed in plan view, oscillatory ripple forms are characterised by bifurcating crests and display interference patterns (Fig. 5D and E). Brecciated aeolian sandstones (Ab) are usually observed as metre-scale polygonal fracture fill networks (see Fig. 4B and C in Hême de Lacotte *et al.*, 2026) penetrating underlying heavily deformed aeolian cross-stratification sets (Axs/Atxs; Fig. 5F). Aeolian dune intraclasts, ranging from pebble to boulder size, are observed sporadically within the sandy matrix of fracture fills (Fig. 5A and B).

© 2026 The Author(s). *Sedimentology* published by John Wiley & Sons Ltd on behalf of International Association of Sedimentologists, *Sedimentology*, **73**, 2081–2119

13653091, 2026, 6, Downloaded from https://onlinelibrary.wiley.com/doi/10.1111/sed.70126 by British Geological Survey, Wiley Online Library on [15/10/2026]. See the Terms and Conditions (https://onlinelibrary.wiley.com/terms-and-conditions) on Wiley Online Library for rules of use; OA articles are governed by the applicable Creative Commons License

Interpretation. Extensive units of mixed aeolian and subaqueous facies are interpreted as coastal dunes that were highly influenced by tidal and wave dynamics and deposited under very high water table conditions associated with rapid subsidence rates. Cross-stratified to structureless sandstones (Mxs) are attributed to variable subaqueous transport styles during tidal breaching and reworking of isolated barchans in back-barrier settings (Fryberger *et al.*, 1983, 1990; Rodríguez-López *et al.*, 2012). Cross-stratified sets and plane beds are associated with subaqueous dune migration and lower regime sediment transport by laminar flow while structureless deposits are deposited by non-Newtonian sediment-saturated flows. Despite their aeolian textural character, Mxs cross-stratification sets cannot be assigned to subaerial dune migration processes due to their relatively small preserved thicknesses. Furthermore, the association of cross-stratification sets, plane beds and structureless units translate the highly variable state of current conditions, a character restricted to subaqueous settings. Other observations suggesting a lack of subaerial processes include (i) numerous convolute lamination structures indicating early dewatering-induced deformation of sediments and (ii) absent reverse grading within foreset grainflow deposits. Oscillatory rippled aeolian sandstones (Mwr) are interpreted as the product of wave reworking of aeolian dune sediments in shallow tidal ponds (e.g. Kocurek, 1981; Blakey & Middleton, 1983; Chan, 1989). Brecciated aeolian sandstones (Ab) were developed on evaporitic crusts that were subject to surficial groundwater salt precipitation, which ultimately led to the formation of large polygonal fractures gradually filled with subsequent windblown sediment (*sensu* Kocurek & Hunter, 1986; Lokier, 2012; Falkenberg *et al.*, 2025). Coupled with the development of subaqueous cross-strata (Mxs), such surfaces are interpreted as aeolian deflationary super surfaces (Fryberger *et al.*, 1988; Havholm & Kocurek, 1994).

Supratidal flat element (M2)

Description. Elements of this type are characterised by tabular bodies and are mostly defined by very fine-grained lithofacies (Fig. 7). They range from 1 to 5 m in thickness and are usually correlatable over several kilometres. They can be interbedded with sub- to intertidal flat elements (M3) and typically truncate marginal aeolian elements (A1, M1; Figs 3, 11A and 12B). They are mostly observed in marginal sections of the study area, although very rare occurrences have been recorded in erg-centre regions (Fig. 3). These elements are dominated by poorly stratified red siltstone and mudstone (Mred), often developing extreme desiccation cracks presenting metre-thick fan-like sandy in-fills towards their top surfaces (Fig. 6D). Lens-shaped to laterally continuous beds of cyclically bedded crystallised evaporite deposits (Mgy; Fig. 6A and B) characterised by internal enterolithic folds are observed with wavy to crinkly laminated sets of dolomicritic mudstone and very fine-grained sand couplets (Mmi; Fig. 6C and E). Occurrences of extensive (ca. >100 m long) metre-thick contorted and bleached sandstone units (Aco) are occasionally observed (Fig. 6G).

Interpretation. Elements of this type are interpreted as supratidal flat elements that are comparable to modern coastal sabkha depositional environments (e.g. Alsharhan & Kendall, 2003). Supratidal flats may have developed locally as disconnected ponds (Clement & Holland, 2016) or more extensively as facies belts, both affected by cyclic evaporitic precipitation and sediment layering due to tidal periodicity. The recognition of a process resulting in the deposition of red mudstone beds (Mred) is challenging due to the lack of preserved sedimentary structures. Nevertheless, settling of terrigenous clay and silty material may have occurred in waning flows originating from rare fluvial flooding reaching the coastal plains during the development of the Page erg (Jones & Blakey, 1997). Alternatively, fine sediments could have been derived from windblown material trapped onto dampened surfaces. Crystallised evaporite beds (Mgy) are generated through the interstitial precipitation of gypsum and anhydrite within pore spaces that were affected by groundwater capillary fringes (Kinsman, 1969; Wood & Wolfe, 1969; Kendall, 1978). Wavy to crinkly laminated dolomicritic mudstones (Mmi) are interpreted as tufted microbial mats that were deposited at the transition between intertidal and supratidal zones (Eriksson & Truswell, 1974; Suarez-Gonzalez *et al.*, 2019). Finally, contorted sandstone units (Aco), observed with intense convolute lamination linked to soft sediment deformation of water-saturated siliciclastic bodies, were possibly derived from isolated aeolian bedforms migrating over the supratidal plain (Andreason, 1992) or accumulated coastal sand-sheets.

© 2026 The Author(s). *Sedimentology* published by John Wiley & Sons Ltd on behalf of International Association of Sedimentologists, *Sedimentology*, **73**, 2081–2119

13653091, 2026, 6, Downloaded from https://onlinelibrary.wiley.com/doi/10.1111/sed.70126 by British Geological Survey, Wiley Online Library on [15/10/2026]. See the Terms and Conditions (https://onlinelibrary.wiley.com/terms-and-conditions) on Wiley Online Library for rules of use; OA articles are governed by the applicable Creative Commons License

Sub- to intertidal flat element (M3)

Description. Elements of this type are characterised by extensive kilometre-scale units (Fig. 7) typically interbedded with supratidal (M2) and wave-dominated shoreface to foreshore elements (M4). They are composed of heterolithic flaser-bedded sandstone to lenticular-bedded siltstones (Mht) and are typically observed as relatively thin (1 to 3 m thick) and well stratified units. These elements are characterised by diverse ratios of sand and clay to silt material (Fig. 6F) and present sporadic desiccation cracks. Round-crested oscillatory to current ripple forms of variable migration direction are commonly associated with desiccated clay drapes within their troughs. Rippled surfaces may inconsistently present moderate bioturbation (grade 3 *sensu* Taylor & Goldring, 1993) at specific locations. Occurrences of both carbonate clasts and matrix within this facies have been documented by Hême de Lacotte *et al.* (2026). Plane-bedded marl units (Mma), ranging from 1 to 5 m in thickness, are widely observed in marine-dominated to marginal-erg regions of the study area (Fig. 3). A vertical transition from this element into supratidal elements (M2) is commonly observed.

Interpretation. Elements of this type are interpreted as subtidal to intertidal flat facies belts deposited through differing sedimentary processes of fluctuating energy levels. Heterolithic stratification sets (Mht) record the periodic cyclicity of fluctuations in bed shear stress from ebb-flow currents, active bedload transport and slack tides with resultant clay settlement (Reineck & Wunderlich, 1968). Longer periods of aerial exposure during spring tides led to the formation of desiccation cracks. Variability in ripple morphologies is linked to the high autocyclic nature of tidal flat environments (Chakrabarti, 2005). Deposition of marl units (Mma) is attributed to particles settlement and in-situ carbonate production in very calm and protected

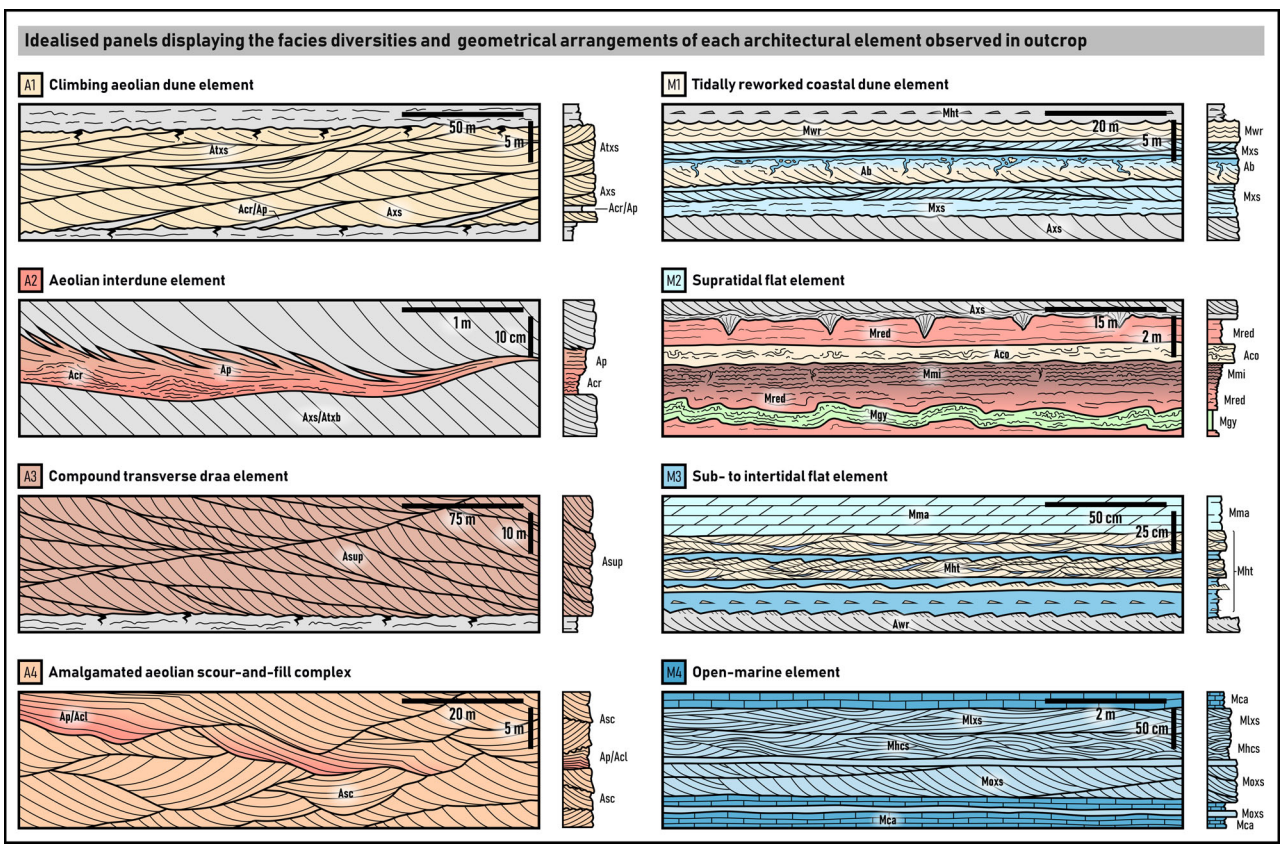

Fig. 7. Architectural elements scheme composed of idealised geometrical arrangements of facies observed in the Temple Cap Formation, Page Sandstone and contemporaneous Carmel Formation. Elements are divided between aeolian (A1 to A4) and shallow-marine primary depositional settings (M1 to M4). Note the significant vertical exaggeration in some panels.

© 2026 The Author(s). *Sedimentology* published by John Wiley & Sons Ltd on behalf of International Association of Sedimentologists, *Sedimentology*, **73**, 2081–2119

13653091, 2026, 6, Downloaded from https://onlinelibrary.wiley.com/doi/10.1111/sed.70126 by British Geological Survey, Wiley Online Library on [15/10/2026]. See the Terms and Conditions (https://onlinelibrary.wiley.com/terms-and-conditions) on Wiley Online Library for rules of use; OA articles are governed by the applicable Creative Commons License

back-barrier lagoons (Riding & Wright, 1981; Steel *et al.*, 2012). While transitions between the two facies were inherited from the irregular spatial distribution of the tidal flat sub-environment, the vertical transitions of this element into supratidal flat elements (M2) is interpreted as shallowing upward sequences.

Open-marine elements (M4)

Description. Elements of this type are characterised by a combination of facies that describe together sediment deposition in the distal-most parts of the study area (Figs 3 and 7). Open-marine elements are mostly composed of metre-thick tabular cosets of cross-stratified oolitic grainstones (Moxs) presenting mud drapes at the toesets of each cross-stratification lamina (see Fig. 11 in Hême de Lacotte *et al.*, 2026). Oolitic grainstones may occur sporadically as plane-bedded sets with lenses of accumulated shelly material. Units of stratified bioclastic wackestone (Mca) are sporadically associated with this element and may display vertical burrows and trace fossils (*Skolithos* and *Cruzania* ichnofacies). Low-angle (Mlxs) and hummocky cross-stratified sandstones (Mhcs) are observed vertically grading into each other (see Fig. 12 in Hême de Lacotte *et al.*, 2026) and are usually interbedded with bioclastic wackestones (Mca) and oolitic grainstones (Moxs).

Interpretation. Elements of this type are interpreted as open-marine facies belts. They are characterised by a wide range of depositional settings and processes in a part of the Carmel Formation system dominated by wave action (Fig. 3; Hême de Lacotte *et al.*, 2026). This variability of observed sedimentary structures and lithologies indicates the coexistence of multiple subaqueous processes associated with variable positions along the shelf. Bioclastic wackestones (Mca) are associated with the deepest settings of the system and are interpreted as facies deposited in the offshore transition zone below the fair-weather base. Cosets of cross-stratified oolitic grainstone (Moxs) are linked to the migration of compound dunes under a tidally modulated current (Gonzalez & Eberli, 1997; Olariu *et al.*, 2012). Wave-dominated shoreface to foreshore transitions were recorded during the migration of barrier islands and are characterised by hummocky cross-stratified sandstones (Mhcs) vertically grading into low-angle cross-stratified sandstones (Mlxs; McCubbin, 1982; Dalrymple & Rivers, 2023).

SPATIO-TEMPORAL CHARACTER AND EVOLUTION IN SEDIMENTARY ARCHITECTURE

Temporal evolution

A stratigraphical framework across the Temple Cap and Page erg margin is reconstructed here, based upon the recognition of key stratigraphical surfaces and their correlation across two transects oriented roughly perpendicular to the Sundance Sea palaeocoastline (Fig. 8). The Temple Cap and Page successions record the deposition of a full T–R sequence with a preferential preservation of the aeolian regressive system tracts. Vertical facies dislocations between aeolian and marine primary depositional settings are used in marginal parts of the system to define composite regressive (CR) and maximum flooding (MF) surfaces. In central-erg regions, deflationary super surfaces are used as inland markers of these key stratigraphical surfaces where both CR and MF surfaces often form compound horizons (Blakey *et al.*, 1996).

This study interprets that early dune field development and deposition of the Temple Cap Formation was preferentially preserved in low palaeotopographical zones of higher accommodation onto the irregular surface of the J-1 Unconformity, with thicknesses reaching up to 35 m (Section 7; Fig. 8B). The subsequent deflation of the Temple Cap Formation dune field and the shaping of its associated composite regressive surface (CR1) are interpreted to have been triggered by the initial relative sea-level rise linked to the Judd Hollow Member transgressive tract. The recorded thickness of the marine Judd Hollow Member dramatically decreases eastward to the point where its associated maximum flooding surface (MF1) is gradually condensed onto the underlying CR1 in central-erg regions. Development of a second and more widespread aeolian sequence was preserved as the Thousand Pockets and Leche-e members. This second erg expansion was punctuated by localised to regional deflationary stages occasionally associated with the deposition of secondary marine units (i.e. the 'upper' Judd Hollow tongue and associated 'S-rm' surface, *sensu* Havholm *et al.*, 1993). Sporadic occurrences of secondary deflationary super surfaces and transgressive packages within regressive system tracts may be interpreted as the expression of a second-order allocyclic signal causing higher frequency fluctuations of relative sea-level or wind seasonality. The termination of the Page erg defines the composite regressive

© 2026 The Author(s). *Sedimentology* published by John Wiley & Sons Ltd on behalf of International Association of Sedimentologists, *Sedimentology*, **73**, 2081–2119

13653091, 2026, 6, Downloaded from https://onlinelibrary.wiley.com/doi/10.1111/sed.70126 by British Geological Survey, Wiley Online Library on [15/10/2026]. See the Terms and Conditions (https://onlinelibrary.wiley.com/terms-and-conditions) on Wiley Online Library for rules of use; OA articles are governed by the applicable Creative Commons License

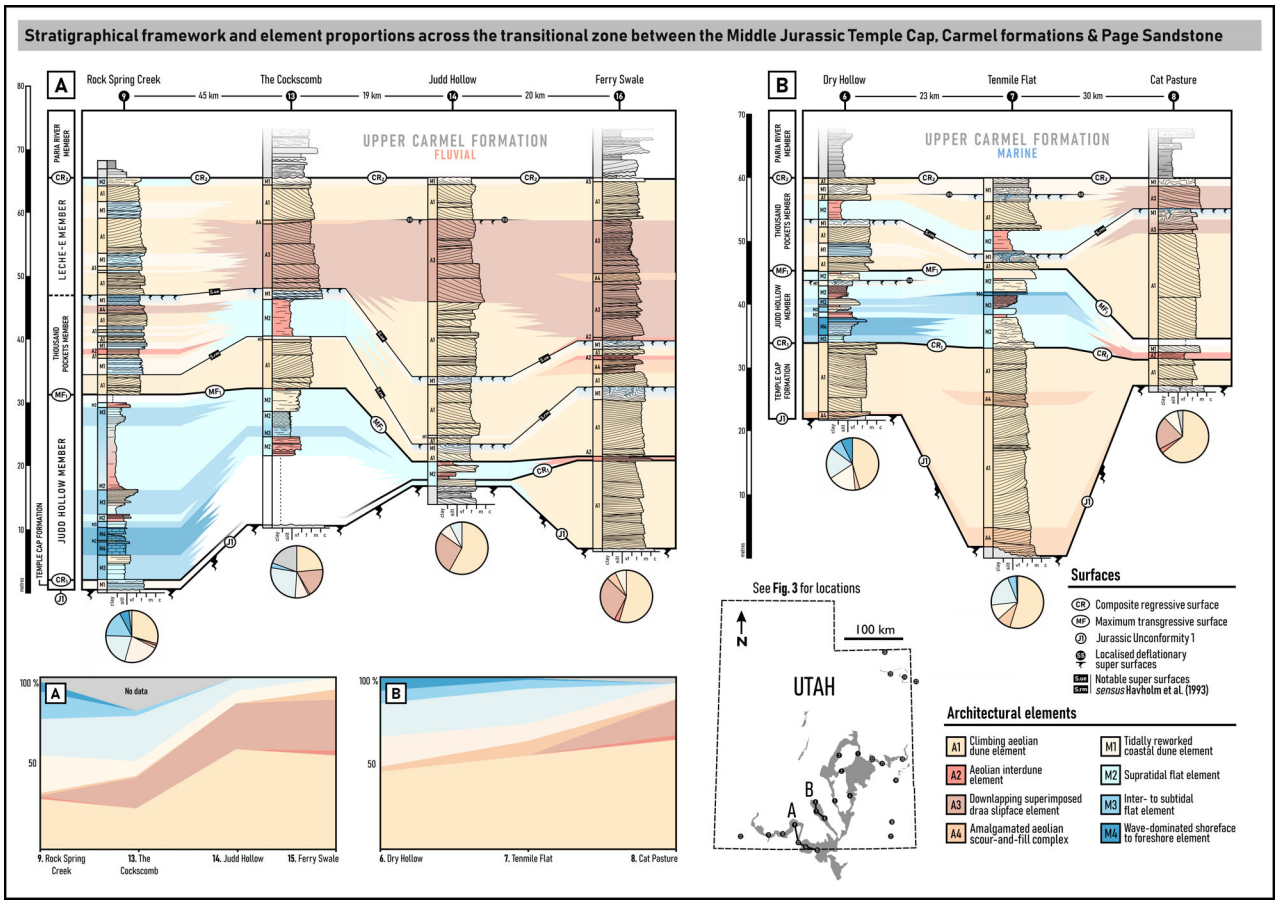

Fig. 8. Regional stratigraphical framework of the Temple Cap Formation, Carmel Formation and Page Sandstone composed of two palaeoshoreline-perpendicular correlation panels depicting the spatio-temporal evolution of architectural elements within system tracts. Architectural element proportions are given for each section.

surface CR2 onto which are unconformably deposited marine to fluvial sediments of the Paria River Member (i.e. informal 'undivided upper' Carmel Formation). This surface corresponds to the 'S-up' super surface from Havholm *et al.* (1993) and was described as a 'minor unconformity' that increases in erosion towards the Monument Upwarp in southeastern regions, areas of geology not investigated in this study. An erosional regime in the dune field during the development of the CR2 surface is observed in the eastern Kaiparowits Plateau, as shown by the absence of the Leche-e Member in this region (Fig. 12B; Havholm & Kocurek, 1994).

Spatial variations

Central-erg (type section: 16 – Ferry Swale & Manson Mesa)

Following the development of regionally correlative sheet-like interdune elements (A2) linked to the Judd Hollow Member transgression (CR1 to MF1), central-erg aeolian parasequences deposited during the regressive system tract in the Page Sandstone are dominated by extensive large-scale compound transverse draa elements (A3) representative of a mature dune field system (Fig. 9). Although associated climbing dune (A1) and interdune elements (A2) are sporadically observed, their scarcity in central-erg regions has been associated to the latter reworking of early dune field bedforms by larger draa (Cardenas *et al.*, 2019; Swanson *et al.*, 2019), which implies an incomplete stratigraphical record in central-erg regions (i.e. Kocurek & Day, 2018). Nevertheless, sets of simple climbing dune elements (A1) are sporadically recorded interbedded within compound draa cosets (A3). Erg termination of the Page Sandstone in central-erg regions (CR2) is expressed by the deposition of an erosive complex (i.e. belt) of amalgamated aeolian scour-and-fill

© 2026 The Author(s). *Sedimentology* published by John Wiley & Sons Ltd on behalf of International Association of Sedimentologists, *Sedimentology*, **73**, 2081–2119

13653091, 2026, 6, Downloaded from https://onlinelibrary.wiley.com/doi/10.1111/sed.70126 by British Geological Survey, Wiley Online Library on [15/10/2026]. See the Terms and Conditions (https://onlinelibrary.wiley.com/terms-and-conditions) on Wiley Online Library for rules of use; OA articles are governed by the applicable Creative Commons License

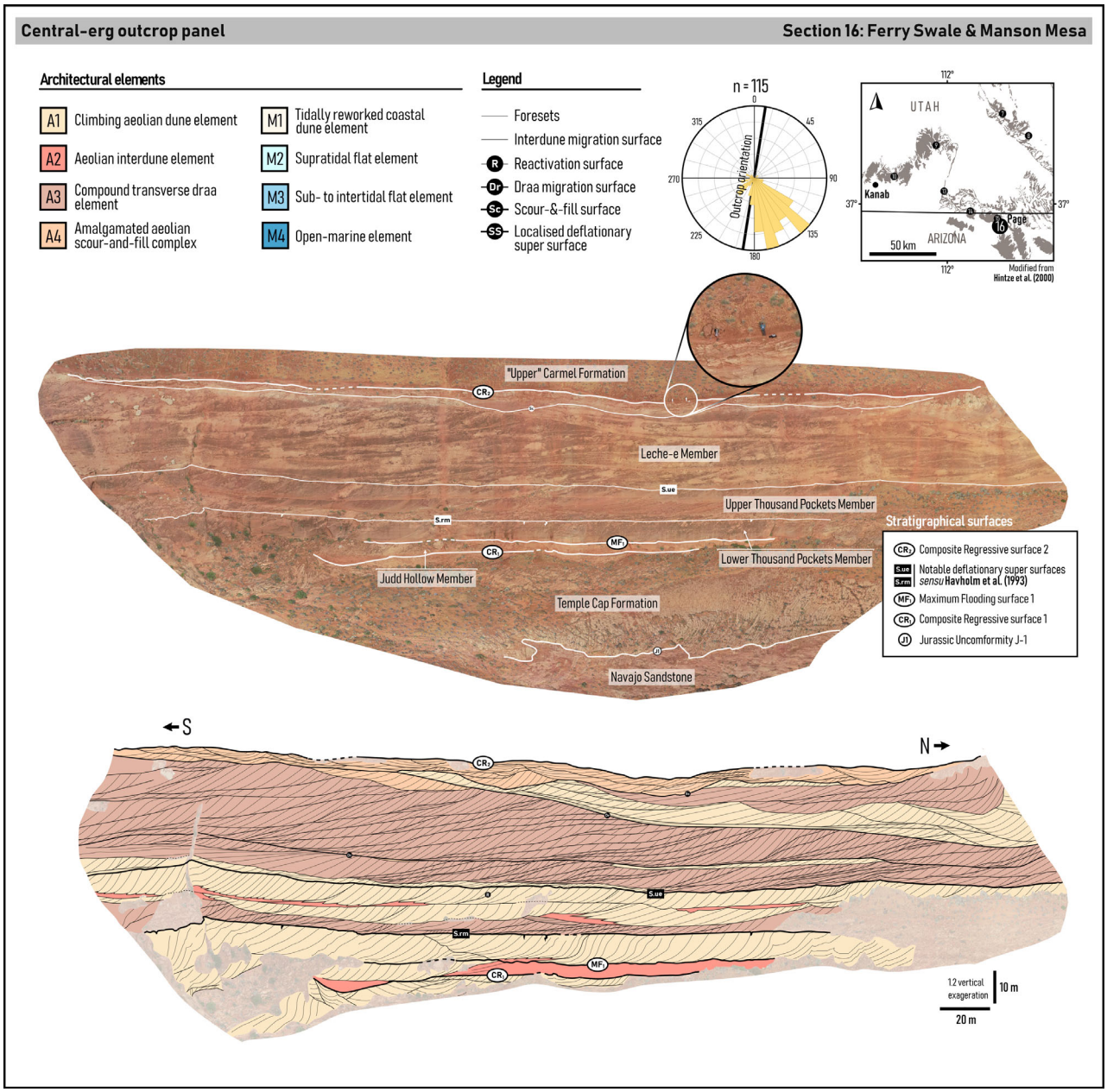

Fig. 9. Outcrop panel displaying architectural elements geometries and relationships in central-erg regions of the Temple Cap Formation and Page Sandstone (Section 16: Ferry Swale & Manson Mesa) with annotated bounding surfaces and palaeocurrent measurements. Central-erg regions are dominated by compound transverse draa elements (A3) and climbing aeolian dune elements (A1). Note the amalgamated scour-and-fill complex (A4) associated with the termination of the Page erg defining the CR2 surface.

sediments (A4). Together, these elements indicate an area of high sediment availability enabling the development of complex superimposed bedforms and the cannibalisation of early dune field growth stages during regressive system tracts.

Medial-erg (type section: 14 – Judd Hollow)

The sedimentary record of the Page Sandstone in medial-erg regions is broadly comparable to central-erg ones, with the only significant difference being the occurrence of supratidal flat elements (M2) deposited during the Judd Hollow

13653091, 2026, 6, Downloaded from https://onlinelibrary.wiley.com/doi/10.1111/sed.70126 by British Geological Survey, Wiley Online Library on [15/10/2026]. See the Terms and Conditions (https://onlinelibrary.wiley.com/terms-and-conditions) on Wiley Online Library for rules of use; OA articles are governed by the applicable Creative Commons License

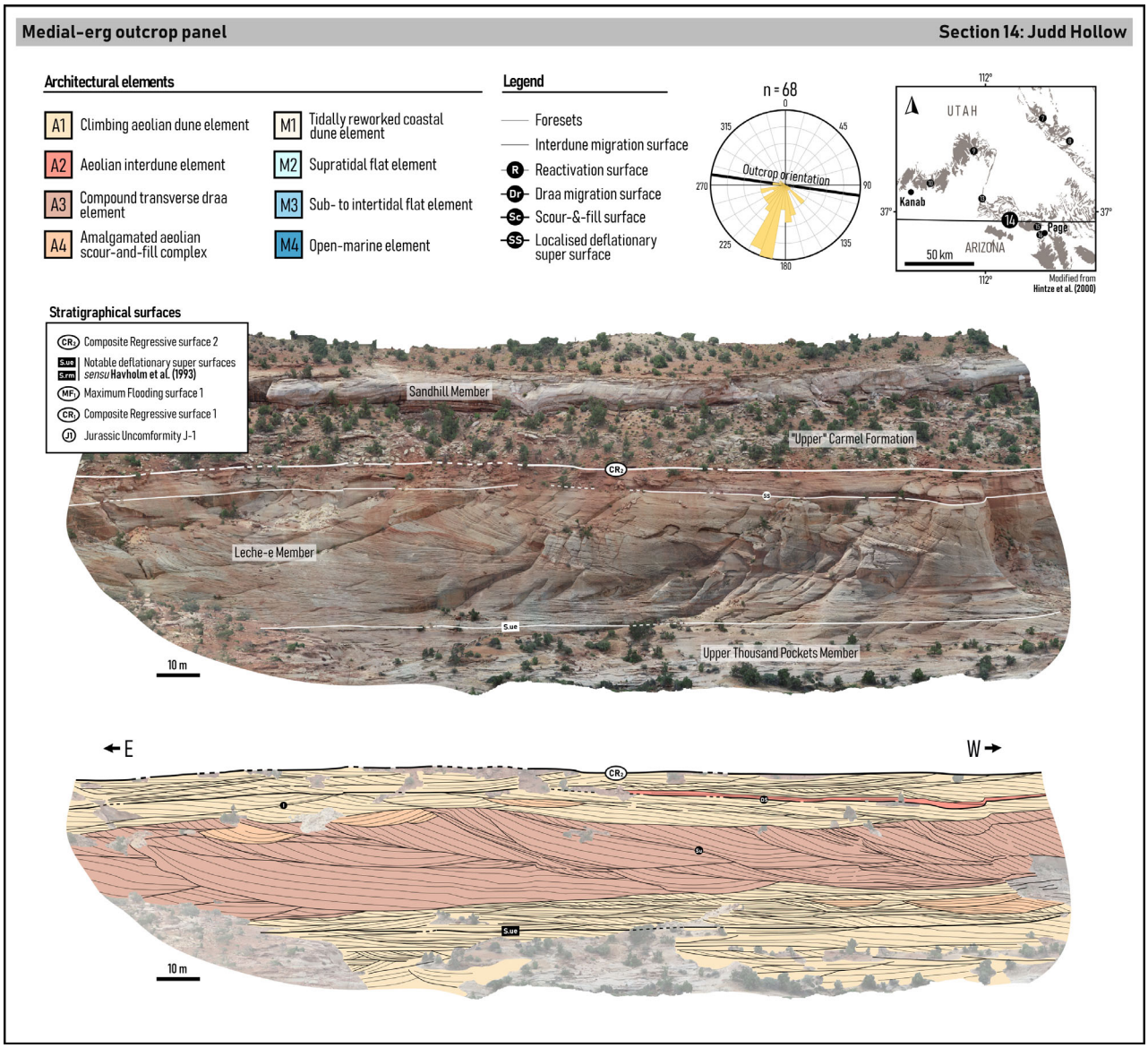

Fig. 10. Outcrop panel displaying architectural elements geometries and relationships in medial-erg regions of the Temple Cap Formation and Page Sandstone (Section 14: Judd Hollow) with annotated bounding surfaces and palaeocurrent measurements. Medial-erg regions are characterised by higher proportions of climbing aeolian dune elements (A1) relative to draa elements (A3). Note the absence of scour-and-fill complexes.

transgression from the northeast (MF1; Fig. 8A). Compound draa cosets (A3) that are stratigraphically equivalent to the ones described in central-erg sections, are present in equal proportion to climbing dune elements (A1; Fig. 10). Erg termination of the Page Sandstone (CR2) is here characterised by the development of a deflationary super surface, which is coupled with the preservation of extensive sheet-like interdune elements (A2) linked to the aggradation of windblown material. Preservation of these deposits was enabled by rising water table dynamics contemporaneous with the deflation event. Together, these elements indicate an area where, although marine sediments are absent, transgressive system tracts can be expressed and preserved as thicker aggrading continental sabkha (as opposed to central-erg regions where transgressive deposits are generally lacking and condense onto CR deflationary super surfaces). Sediment availability was still sufficient to enable compound aeolian bedform generation

13653091, 2026, 6, Downloaded from https://onlinelibrary.wiley.com/doi/10.1111/sed.70126 by British Geological Survey, Wiley Online Library on [15/10/2026]. See the Terms and Conditions (https://onlinelibrary.wiley.com/terms-and-conditions) on Wiley Online Library for rules of use; OA articles are governed by the applicable Creative Commons License

and preservation during the deposition of regressive system tracts.

Marginal-erg (type sections 7 – Tenmile Flat and 13 – the Cockscomb)

Sedimentary architectures assemblages in marginal-erg regions are marked by substantial increases in the proportions of shallow-marine element with respect to aeolian deposits (Figs 11 and 12). Transgressive deposits associated with the Judd Hollow Member are characterised by laterally extensive units of supratidal flat elements (M2) and sub- to intertidal flat elements (M3), which grade laterally into wave-dominated shoreface to foreshore elements (M4) in laterally adjacent open-marine-dominated regions (Sections 6 and 9; Figs 3 and 8). Dune field development associated with the deposition of the Thousand Pockets Member is composed largely of simple climbing dune elements (A1) that occasionally interfinger with restricted interdune elements (A2). This seaward decrease in aeolian bedform complexity translates spatial changes in sediment availability linked to higher coastal water table elevations. Sporadically, tidally reworked coastal dune elements (M1) and, more exceptionally, supratidal flat elements (M2) are observed interbedded with climbing dune elements (A1). This relationship reflects the increasing influence and proximity of shallow-marine processes during the deposition of regressive system tracts. Where preserved (Section 13; Fig. 11), the sedimentary expression of the Leche-e Member is dominated by compound transverse draa elements (A3), which suggest a significant palaeocoastline retreat at the apex of the Page Sandstone erg. Considering that occurrences of such deposits are usually associated with complex systems of compound dunes recording multiple generations of construction under distinct wind regimes (Kocurek & Ewing, 2005), their preservation in such marginal regions may translate a greater expansion of the Page erg during deposition of the Leche-e Member compared to older units. Development of the CR2 surface and associated termination of the Page erg is expressed differently between marginal sections. In section 13, the CR2 surface is recorded as an irregular surface displaying onlapping relationships of younger strata from the Paria River Member of the Carmel Formation (Fig. 11B; Bowler, 2026). This characteristic of the CR2 surface is potentially inherited from preceding aeolian bedforms palaeotopography of the Leche-e Member. In this case, sporadic reworking and rippling of the top of the Page Sandstone is attributed to transgressive ravinement processes from the following sequence. Elsewhere, this surface is defined as a sharp and flattened deflationary super surface (Fig. 12B). Together, these elements indicate an area where shallow-marine transgressive deposits are fully expressed and preserved, and where aeolian regressive deposits are highly reworked by tidal or wave processes.

The Temple Cap and Page system displays typical changes in sedimentary architecture (Figs 9 to 12) and stratigraphical arrangement (Fig. 8) across a relatively short southeast to northwest transect of approximately 85 km (Fig. 3). These changes reflect a transition from central-erg to marginal-erg regions and, ultimately, to the contemporaneous paralic systems of the Carmel Formation. Vertically, Temple Cap and Page successions are defined by clear aeolian sequences genetically linked to, and correlated with, a dynamic T–R sequence framework recorded in the Carmel Formation. Second-order sequences of marine flooding and aeolian encroachment phases are recorded within regressive system tracts and may be related to high-frequency climatic fluctuations as well as autogenic masking mechanisms or along-shore variability.

DISCUSSION

The sediment distribution and inherent stratal arrangement associated with the development of

Fig. 11. Outcrop panel displaying architectural elements geometries and relationships in marginal-erg regions of the Temple Cap Formation and Page Sandstone (Section 13: The Cockscomb) with annotated bounding surfaces and palaeocurrent measurements. (A) Despite presenting similarities with medial-erg settings (e.g. correlative draa elements present in the Leche-e Member), marginal-erg regions predominantly display climbing aeolian dune elements (A1) interbedded with tidally reworked coastal dune elements (M1) and marine elements (M2 to M4). (B) Annotated photograph displaying the localised unconformable relationship between the aeolian Leche-e Membre and the overlying fluvial deposits of the Paria River Member highlighting the uneven erosion and the time hiatus locally characteristic of the CR2 surface development. Note the rippled surface linked to the reworking of underlying aeolian dune material.

© 2026 The Author(s). *Sedimentology* published by John Wiley & Sons Ltd on behalf of International Association of Sedimentologists, *Sedimentology*, **73**, 2081–2119

13653091, 2026, 6, Downloaded from https://onlinelibrary.wiley.com/doi/10.1111/sed.70126 by British Geological Survey, Wiley Online Library on [15/10/2026]. See the Terms and Conditions (https://onlinelibrary.wiley.com/terms-and-conditions) on Wiley Online Library for rules of use; OA articles are governed by the applicable Creative Commons License

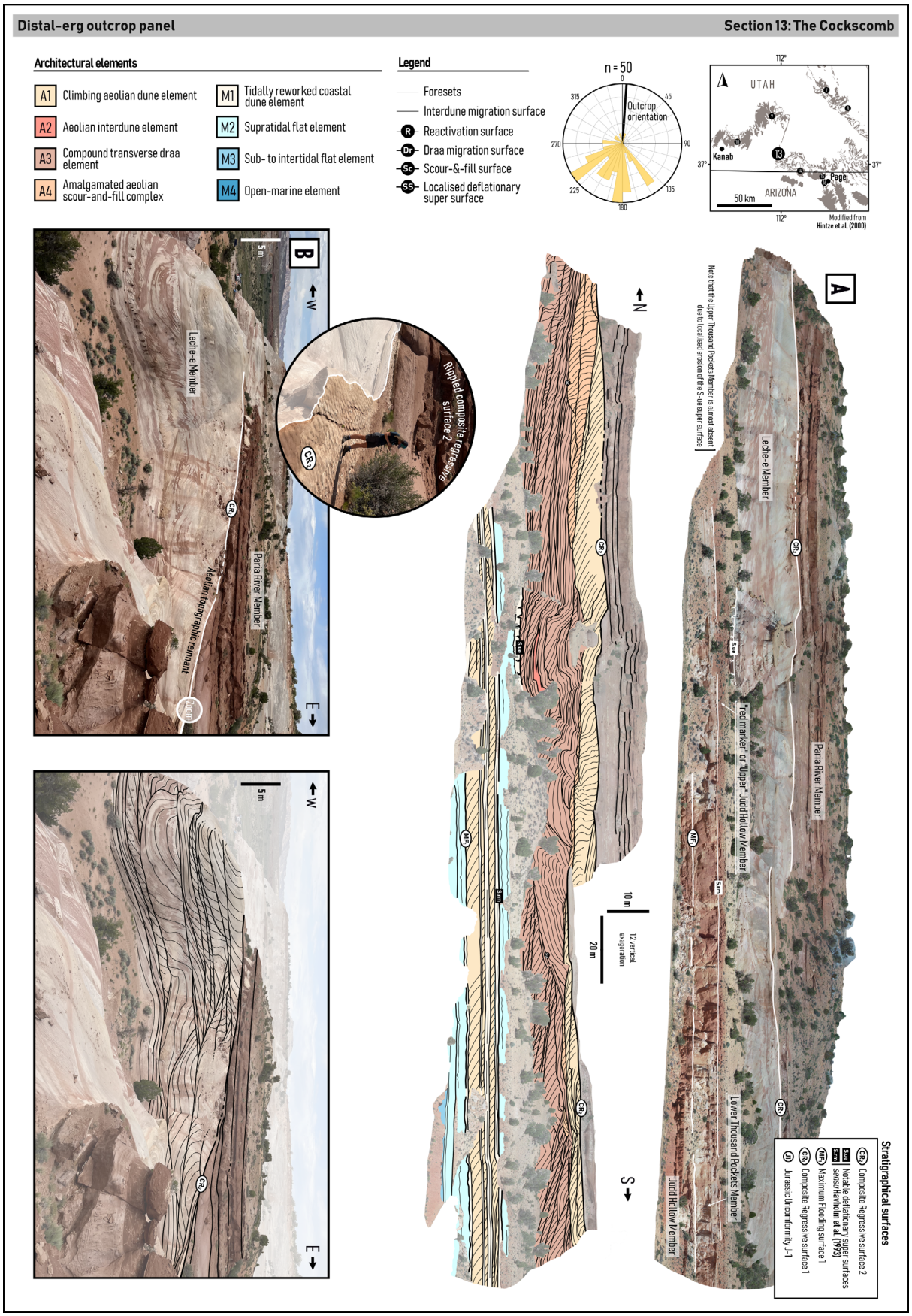

© 2026 The Author(s). *Sedimentology* published by John Wiley & Sons Ltd on behalf of International Association of Sedimentologists, *Sedimentology*, **73**, 2081–2119

13653091, 2026, 6, Downloaded from https://onlinelibrary.wiley.com/doi/10.1111/sed.70126 by British Geological Survey, Wiley Online Library on [15/10/2026]. See the Terms and Conditions (https://onlinelibrary.wiley.com/terms-and-conditions) on Wiley Online Library for rules of use; OA articles are governed by the applicable Creative Commons License

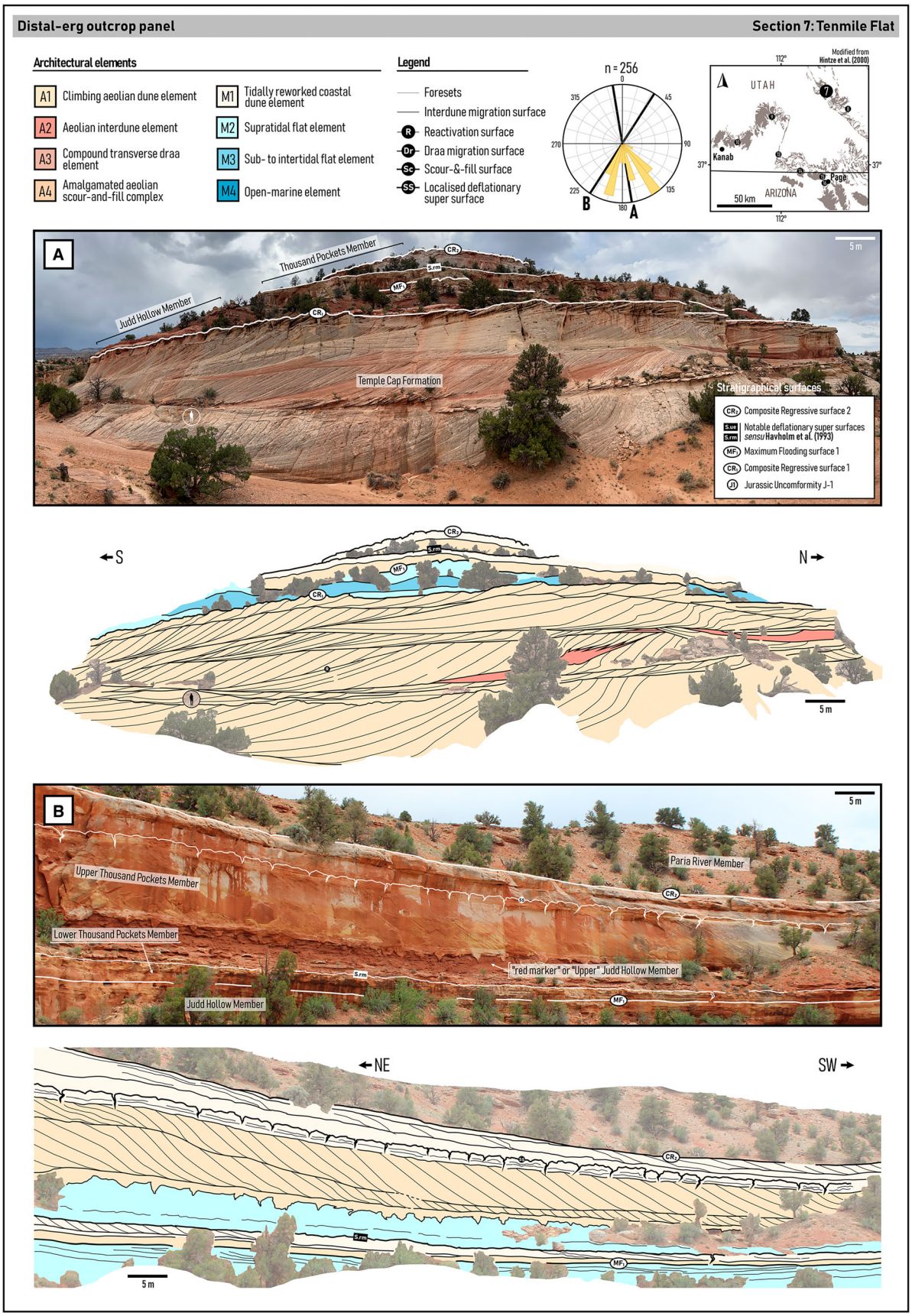

© 2026 The Author(s). *Sedimentology* published by John Wiley & Sons Ltd on behalf of International Association of Sedimentologists, *Sedimentology*, **73**, 2081–2119

13653091, 2026, 6, Downloaded from https://onlinelibrary.wiley.com/doi/10.1111/sed.70126 by British Geological Survey, Wiley Online Library on [15/10/2026]. See the Terms and Conditions (https://onlinelibrary.wiley.com/terms-and-conditions) on Wiley Online Library for rules of use; OA articles are governed by the applicable Creative Commons License

Fig. 12. Outcrop panel displaying architectural elements geometries and relationships in marginal-erg regions of the Temple Cap Formation and Page Sandstone (Section 7: Tenmile Flat) with annotated bounding surfaces and palaeocurrent measurements.

aeolian–marine margins, as discussed by pre-existing models (Blakey *et al.*, 1996; Jordan & Mountney, 2012; Rodríguez-López *et al.*, 2013; Blanchard *et al.*, 2016), have been attributed previously to alternating coastal-fed dune field encroachments and shallow-marine dispersal of aeolian deposits. When coupled together, these successions may be used to define a sequential T–R framework, with aeolian and marine strata being preferentially deposited and preserved during RST and TST, respectively. Numerous studies have revealed differing styles of coastal erg termination in response to transgressive mechanisms (Eschner & Kocurek, 1986; Ahmed Benan & Kocurek, 2000; Kocurek *et al.*, 2019; Paz *et al.*, 2021) or sediment shutdown scenarios (Cross *et al.*, 2023). Although well-documented case-specific models exist, spatial complexities in sedimentary architectures and the expressions of stratigraphical surface are yet to be emphasised.

Middle Jurassic palaeogeography of the Utah-Idaho Trough

This study proposes regional palaeogeographical reconstructions depicting spatial arrangements of contemporaneous marine and aeolian systems. These reconstructions demonstrate that several erg development sequences were recorded in the Temple Cap Formation and Page Sandstone at different temporal scales. Transitional zones between both depositional environments reveal changes in scales and facies proportions linked to progressive shifts in dominant autogenic surfaces processes, preservation potential and overarching allogenic controls, which jointly lead to complexities in stratigraphical architectures. Basin-scale palaeogeographical analysis for key stratigraphical time surfaces provides means of discussing the wider environmental changes affecting the Temple Cap and Page erg (and contemporaneous units).

Early dune field development phase and transgression initiation – CR1 (ca. 170 ma)

Following a depositional hiatus characterised by the J-1 Unconformity, the uneven preservation of aeolian strata from the Temple Cap Formation is considered to reflect the influence of palaeotopographical variability onto its stratigraphical record. These deposits were bordered by the supratidal deposits of the Manganese Wash Member towards Saint George (Sprinkel *et al.*, 2011) and the Gypsum Spring Formation in Wyoming and Idaho (Clement & Holland, 2016). Stratigraphical and palynological investigations coupled with $^{40}Ar/^{39}Ar$ (sanidine) and U–Pb (zircon) radiochronological analyses of ash layers (Kowallis *et al.*, 2001; Dickinson *et al.*, 2010; Sprinkel *et al.*, 2024) suggest that the transgression of the primordial Sundance Sea was initiated from two opposite sources. Marine sediment distribution was then mainly controlled by the presence of physical barriers, such as topographical palaeohighs which prevented marine flooding from propagating into the Utah-Idaho Trough (e.g. Ancestral Uinta Mountains). Fluvial sediments from the Rone Bailey Member in the region of Moab are interpreted as runoffs from Uncompahgre remnants and other local unnamed highs.

The CR1 surface is linked to the process causing the widespread deflation of the isolated coastal dune fields defining the Temple Cap Formation. Figure 13A illustrates the facies distribution associated with this key time surface and thus depicts the maximum preserved extent of the Temple Cap Formation erg based on exposed sediments (maximum deposited erg extent remains unknown due to later erosion during deflation).

Maximal marine transgression and tidal embayment – MF1 (ca. 167.7 ma)

Regional flooding of the Sundance Sea during Bajocian times was recorded by multiple marine deposits ranging from offshore sediments of the Arapien Formation (Picard & Uygur, 1982) in western Utah, carbonate ramp successions of the Twin Creek Limestone (Sprinkel, 1982) in Wyoming and the Co-op Creek Member in southwestern Utah, and coastal to supratidal sediments of the Judd Hollow Member in central Utah (Hême de Lacotte *et al.*, 2026). Although sporadic occurrences of tidally-reworked aeolian

© 2026 The Author(s). *Sedimentology* published by John Wiley & Sons Ltd on behalf of International Association of Sedimentologists, *Sedimentology*, **73**, 2081–2119

13653091, 2026, 6, Downloaded from https://onlinelibrary.wiley.com/doi/10.1111/sed.70126 by British Geological Survey, Wiley Online Library on [15/10/2026]. See the Terms and Conditions (https://onlinelibrary.wiley.com/terms-and-conditions) on Wiley Online Library for rules of use; OA articles are governed by the applicable Creative Commons License

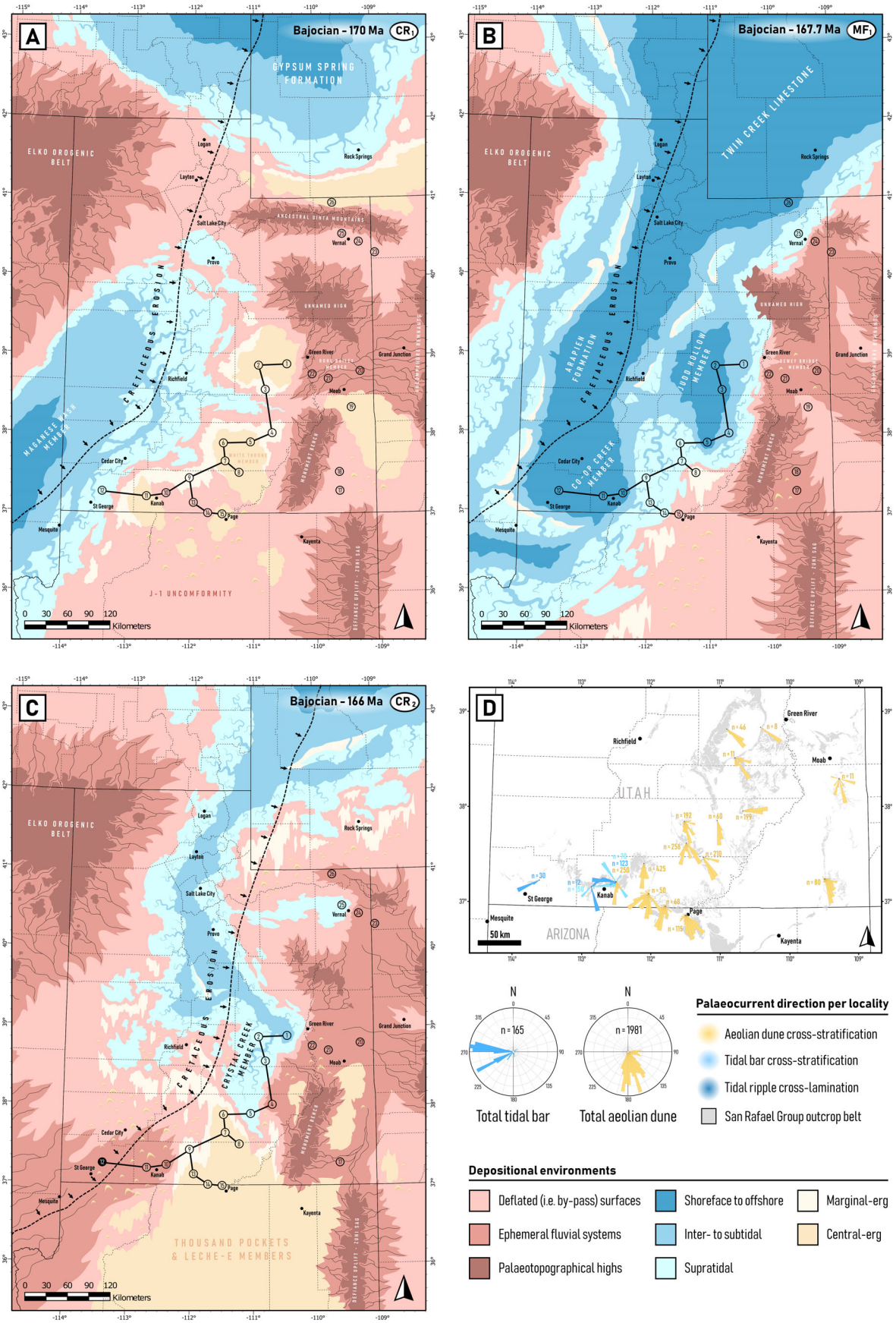

13653091, 2026, 6, Downloaded from https://onlinelibrary.wiley.com/doi/10.1111/sed.70126 by British Geological Survey, Wiley Online Library on [15/10/2026]. See the Terms and Conditions (https://onlinelibrary.wiley.com/terms-and-conditions) on Wiley Online Library for rules of use; OA articles are governed by the applicable Creative Commons License

Fig. 13. Palaeogeographical reconstruction maps of the Utah-Idaho Trough for three key sequence-stratigraphical surfaces CR1 (A), MF1 (B) and CR2 (C). (D) Map displaying palaeocurrent data from preserved aeolian (yellow) and tidal (blues) dune foreset azimuths at different localities across the studied area (outcrop belt extent derived from Hintze *et al.*, 2000).

strata were present in southern Utah, most of the Page erg was undergoing a regional deflationary stage or bedform by-pass triggered by low sediment availability conditions preventing dune field climb. High elevations of the inland water table leading to coastal sabkha aggradation are thought to be directly linked to the relative sea-level dynamics of the Sundance Sea (Kocurek *et al.*, 2001). Fluvial runoff from the various palaeotopographical highs is recorded in the region of Moab and Bluff (e.g. Dewey Bridge Member). The MF1 surface is linked to the regional flooding of the Sundance Sea. Figure 13B illustrates the facies distribution associated with this key time surface and depicts the maximum flooding extent of the Judd Hollow Member and contemporaneous lithostratigraphical units based on exposed sediments.

Aridity maximum and erg development apex – CR2 (ca. 166 ma)

Regional retreat of the Sundance Sea was associated with the deposition of regressive supratidal sediments in regions of high accommodation conditions (e.g. Green River region) and the progradation of ephemeral fluvial systems near topographical highs (e.g. Kanab region). Together, these deposits define the Crystal Creek Member of the Carmel Formation. Concomitantly to this regression, aeolian depositional sequences of the Thousand Pockets and Leche-e members were developing under a southward-dominant palaeowind regime across a broad region in southern Utah and northern Arizona (Fig. 13D). Although unknown amounts of strata of the Page Sandstone were unevenly eroded away by the widespread deflationary event linked to the CR2 surface ('S-up', *sensu* Havholm *et al.*, 1993), the observed extent of aeolian deposits may be used to define a maximum preserved erg development area (i.e. apex). It is evident that the final deflation of the Page erg was initiated in part by the onset of a second T–R sequence with the regional flooding indicated by sediments of the Paria River Member and the development of contemporaneous fluvial systems (cf. Bowler, 2026). However, the uneven erosion of the Page Sandstone sequences cannot be explained solely by changes in levels of the water table and associated sediment availability. Instead, development of the CR2 could result in part from localised changes in base levels due to bulging in the Monument Upwarp area on which the Page dune field was flanked. Figure 13C illustrates the facies distribution associated with this key time surface and depicts the joint maximum regressive extent of the Crystal Creek Member and the erg apex of the Page Sandstone (Thousand Pockets and Leche-e members combined).

Palaeoclimatic setting

Lower to Middle Jurassic aeolian successions of the Colorado Plateau are generally associated to significant wind seasonality linked to monsoonal atmospheric circulations across the western Pangea margin, in palaeolatitudes ranging from 20° to 25°N (Loope *et al.*, 2001). Alternating dominant northwesterly winds and secondary northeasterly trade winds have been interpreted from aeolian strata of the Navajo Sandstone underlying the Temple Cap Formation (Parrish & Peterson, 1988; Peterson, 1988). Aeolian palaeocurrent data of the Temple Cap and Page erg collected in this study collectively suggest that northwesterly trending wind conditions continued throughout the deposition of these units (Fig. 13D). Spatial analysis of measured palaeocurrent data reveals significant variability in the mean directions of bedform foreset azimuths at each locality, which can be linked to bedform complexity and/or measurement bias.

Although a significant part of the Temple Cap and Page erg is composed of recycled material from the underlying Navajo Sandstone (Dickinson & Gehrels, 2009), southward sediment transport from the Sundance Seaway shoreline must have provided significant amounts of detrital products to the system (Peterson, 1988). Shallow-marine sediments of the contemporaneous Carmel Formation were deposited in a dynamic setting of alternating shoreline

© 2026 The Author(s). *Sedimentology* published by John Wiley & Sons Ltd on behalf of International Association of Sedimentologists, *Sedimentology*, **73**, 2081–2119

13653091, 2026, 6, Downloaded from https://onlinelibrary.wiley.com/doi/10.1111/sed.70126 by British Geological Survey, Wiley Online Library on [15/10/2026]. See the Terms and Conditions (https://onlinelibrary.wiley.com/terms-and-conditions) on Wiley Online Library for rules of use; OA articles are governed by the applicable Creative Commons License

progradation and retrogradation (Blakey *et al.*, 1996; Hême de Lacotte *et al.*, 2026). This implies that dune field development phases of the Temple Cap and Page system, and the preservation of their associated aeolian sequences, were most likely controlled by periodic shutdowns and reactivations of coastal sediment sources.

Spatial complexity of coastal erg margins

Changes in aeolian architectures across the erg margin of the Page Sandstone are indicative of a coastal dune field experiencing a periodicity in development stages and a seaward sediment deficit along its extent. As depicted in Fig. 14, mature coastal ergs may be subdivided into three arbitrary sub-depositional belts indicative of a regressive system tract: (i) central-erg; (ii) medial-erg; (iii) marginal-erg. Due to their high sediment availability, central-erg regions (Fig. 14C) present sedimentary architectures characteristic of a well-developed field of compound transverse draas (A3). Unless developed in a basin undergoing sufficient and constant accommodation creation for steady bedforms to climb (i.e. rapidly subsiding basin *sensu* Cosgrove *et al.*, 2022), sediments from early dune field growth phases in central-erg regions will tend to be remobilised by such large bedforms (Swanson *et al.*, 2019). Medial-erg regions (Fig. 14B) demonstrate the architectural characteristics of a wet aeolian system (*sensu* Kocurek & Havholm, 1993) with a higher proportion of simple climbing transverse dune (A1) and interdune elements (A2). Medial-erg depositional belts are indeed more affected by near-surface water table conditions due to their relative proximity with the marine realm (Kocurek *et al.*, 2001). Relatively high moisture conditions will tend to reduce the sediment availability required for compound bedform generation (Mountney, 2012) as well as the preservation potential of each of the dune sets. Marginal-erg regions (Fig. 14A) are defined by complex architectural arrangements symptomatic of a mixed

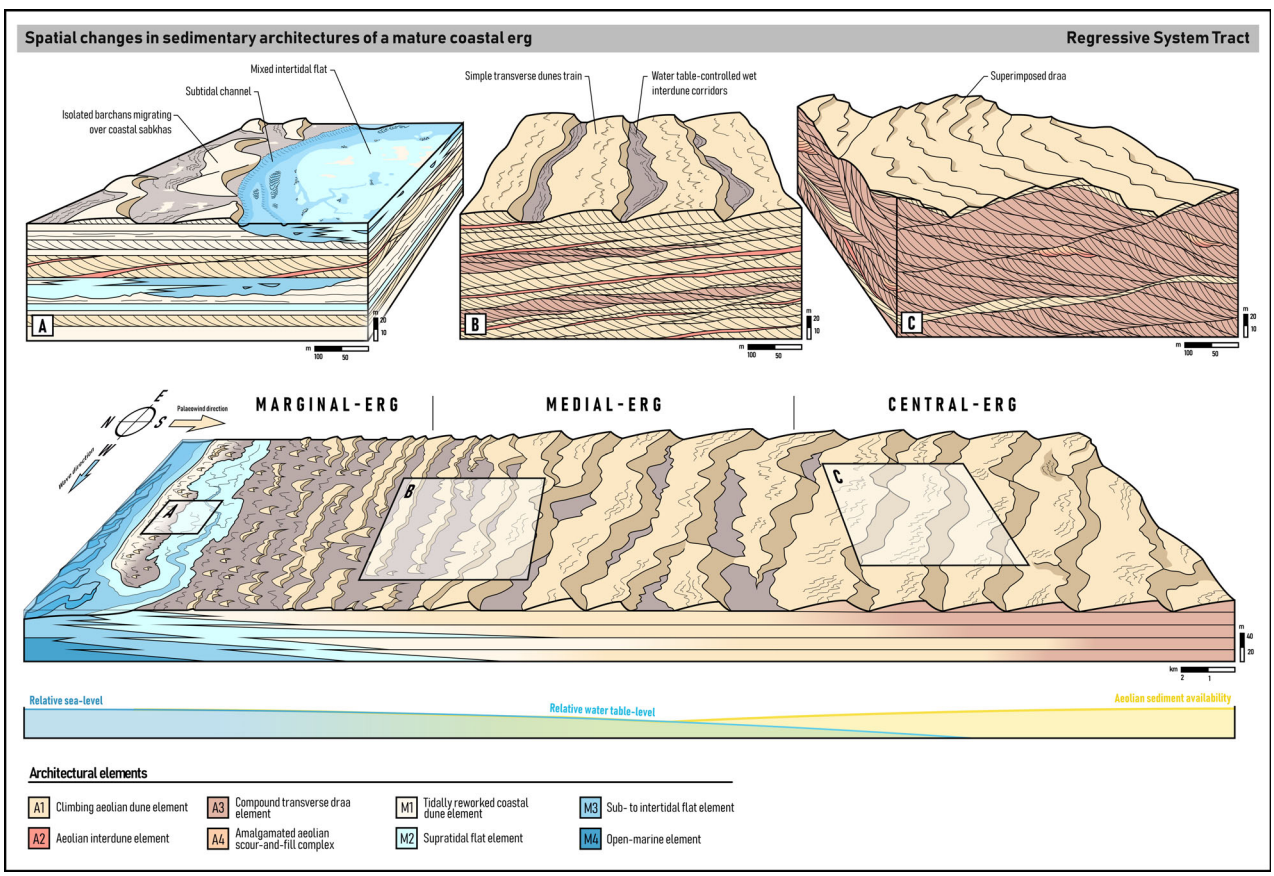

Fig. 14. Depositional model of a mature coastal erg system associated with the development of a regressive system tract. Detailed facies for three depositional belts are given for (A) marginal-erg, (B) medial-erg and (C) central-erg.

13653091, 2026, 6, Downloaded from https://onlinelibrary.wiley.com/doi/10.1111/sed.70126 by British Geological Survey, Wiley Online Library on [15/10/2026]. See the Terms and Conditions (https://onlinelibrary.wiley.com/terms-and-conditions) on Wiley Online Library for rules of use; OA articles are governed by the applicable Creative Commons License

depositional belt affected by constant sediment reworking due to the interplay between tide, wave and aeolian processes (i.e. Rodríguez-López *et al.*, 2012). Complex plan view distributions and strong autogenic overprints in marginal-erg regions will tend to generate unpredictable stratigraphical successions (Zuchuat *et al.*, 2019a; Hême de Lacotte *et al.*, 2026). They are generally composed of climbing aeolian dune cosets (A1) regularly reworked into subaqueous deposits (M1) and interbedded with supratidal flats (M2) and sub- to intertidal flat elements (M3).

In a transgressive setting, flooded coastal ergs may undergo aeolian deflationary stages across their extent. Resulting composite regressive surfaces (CR) may be expressed and recorded differently between each depositional belts: (i) scour-and-fill belts; (ii) deflationary super surfaces and aggrading sabkha; (iii) transgressive ravinement surfaces and tidal embayment. Together, these depositional belts are indicative of a transgressive system tract (Fig. 15). Despite dramatic decreases in aeolian sediment availability due to rising sea-level and associated water table dynamics, self-sustained active dune fields may subsist in the continental-most regions of the erg. Subsisting dune fields in central-erg regions (Fig. 15C) are dominantly recorded as belts (i.e. complexes) of self-reworking scour-and-fill elements (A4) which have the potential to erase significant amounts of aeolian stratigraphical record (Cardenas *et al.*, 2019). The base of these units defines an erosive scour-and-fill surface (CR_{sfs}). Architectural expression of deflated sabkhas in medial-erg regions (Fig. 15B) and their associated deflationary super surface (CR_{dss}) depends on water table dynamics at the time of the deflation (Havholm & Kocurek, 1994). Rising water tables will lead to the preservation of sheet-like aggrading interdune elements (A2) while stationary water tables will generate

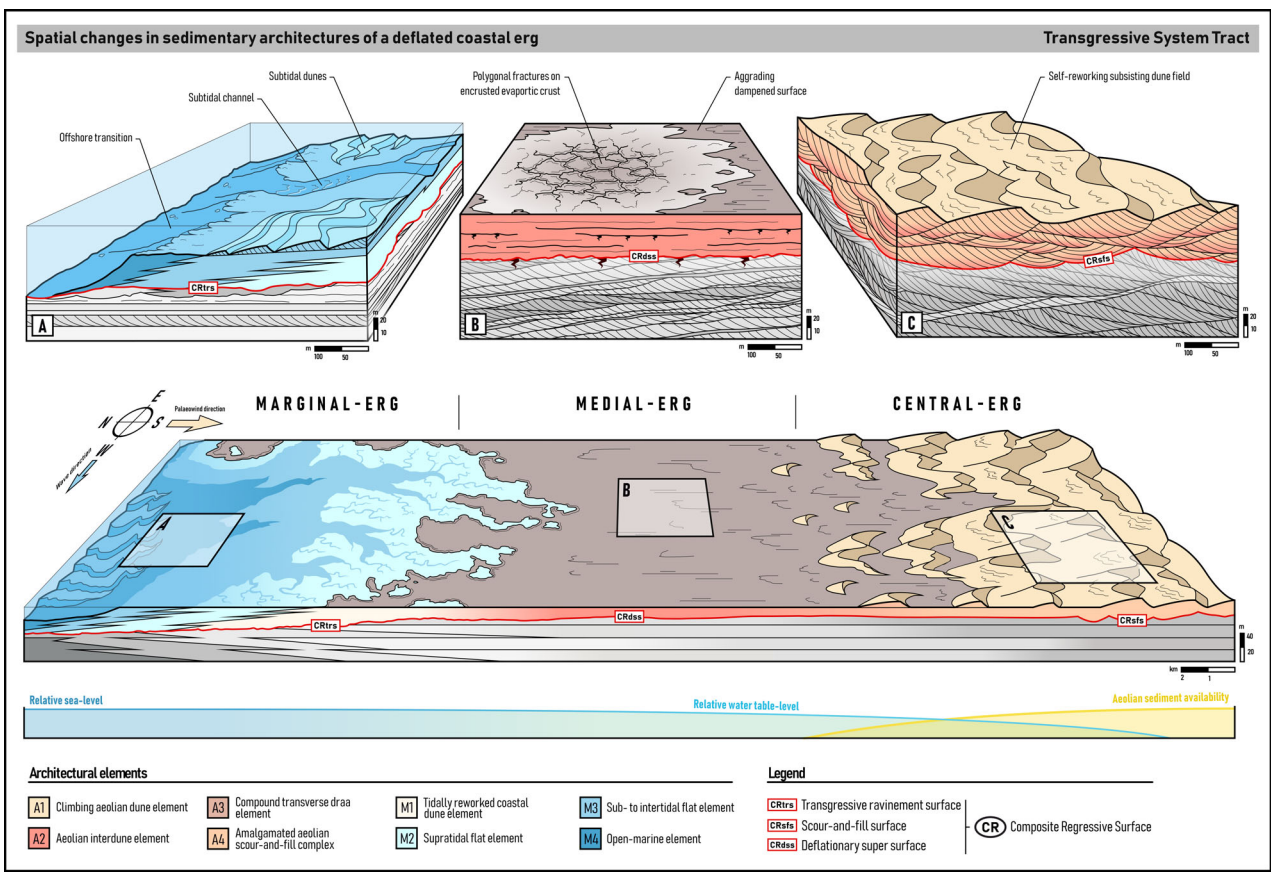

Fig. 15. Depositional model of a flooded coastal erg system associated with the development of a transgressive system tract. Detailed facies for three depositional belts are given for (A) marginal-erg, (B) medial-erg and (C) central-erg. Note the differential expression of the composite regressive surface (CR) across the coastal erg transition.

© 2026 The Author(s). *Sedimentology* published by John Wiley & Sons Ltd on behalf of International Association of Sedimentologists, *Sedimentology*, **73**, 2081–2119

13653091, 2026, 6, Downloaded from https://onlinelibrary.wiley.com/doi/10.1111/sed.70126 by British Geological Survey, Wiley Online Library on [15/10/2026]. See the Terms and Conditions (https://onlinelibrary.wiley.com/terms-and-conditions) on Wiley Online Library for rules of use; OA articles are governed by the applicable Creative Commons License

extensive super surfaces sporadically associated with polygonal fractured evaporitic crusts depending on surface moisture conditions (Kocurek & Hunter, 1986). Falling water table stages will tend to enable the erosion of underlying aeolian strata. Only rising dynamics will lead to the deposition and preservation of sediments as depicted by Fig. 15B. Both CR_{sfs} and CR_{dss} are comparable to subaerial unconformities (SU) in Embry (2010)'s model. Tidal embayments in marginal-erg regions (Fig. 15A) form in a depositional belt where most of the sediment deposition occurs in transgressive settings due to accommodation creation by relative sea-level rise. In such settings, the landward migration of shallow-marine processes leads to the erosion of previously deposited RST strata and the generation of a transgressive ravinement surface (CR_{trs}) which expression may vary spatially (Kirkham, 1997; Zuchuat *et al.*, 2019b). Sedimentary architectures arrangements in tidal embayment regions are characterised by retrograding packages of supratidal flat (M2), inter- to subtidal flat (M3) and shoreface to foreshore elements (M4).

In coastal settings, periodic phases of dune field growth and deflation are primarily caused by changes in sediment availability, although local variations in palaeogeography may influence their preservation potential. Inland rises of water table levels, triggered by marine transgressions will tend to reduce sediment mobility on the depositional surface and can ultimately lead to the development of deflationary super surfaces. Overarching allogenic controls onto their development and the associated termination of aeolian sequences may be linked to orbitally induced shifts in climatic belts (Jordan & Mountney, 2012; Rodríguez-López *et al.*, 2012; Button *et al.*, 2026; Cousins *et al.*, 2026) or tectonically driven shifts in basin subsidence (Cosgrove *et al.*, 2023). We propose that the timing between the development of such surfaces and the deposition of transgressive system tracts is not simultaneous for scenarios where dune fields are sourced from a coastal system. We suggest instead that a spatio-temporal lag exists, whereby stages of rising sea-level and changes in the associated water table affect the inland aeolian sediment availability prior to the start of shoreline retrogradation and subsequent deposition of transgressive units (Fig. 16). Despite this diachrony, transgressive ravinement surfaces (CR_{trs}), aeolian deflationary super surfaces (CR_{dss}) and aeolian scour-and-fill complex basal surfaces (CR_{sfs}) are all direct or indirect expressions of marine transgression onto coastal ergs. Together, these surfaces define composite regressive surfaces (CR) that may be used for correlations between depositional belts of differing nature, regardless of their triggering mechanism.

Intraformational heterogeneities are increasingly predominant towards the margins of coastal erg systems through spatial variations in sedimentary architectures. Ultimately, facies changes across such transitions may result in the formation of lateral stratigraphical seals through the accumulation of baffles generated by the sedimentary interactions discussed in this study.

CONCLUSIONS

Intrinsic interactions between contemporaneous aeolian and shallow-marine systems may be expressed differentially across the margins of coastal dune fields. Seaward changes in surface processes and allogenic controls tend to promote complex spatial variations in sedimentary architectures and subsequent reservoir heterogeneities. This new analysis investigates the spatial variability in depositional products of an ancient aeolian–marine margin and its temporal evolution by accounting for the compound influences of relative sea-level and water table fluctuations and their differential expressions across transitional depositional environments of such kind.

In coastal settings, aeolian sequences are developed as regressive system tracts when

Fig. 16. Generic model for the generation of composite regressive surface (CR) across coastal erg transitions. (T1) Dune field development stages promoted by high sediment availability conditions and low relative water table levels, predominantly recorded during regressive phases. (T2) Aeolian deflation to the water table level generating a deflationary super surface (CR_{dss}) across the dune field, although a scour-and-fill surface (CR_{sfs}) may concomitantly develop in central regions through bedform self-reworking processes. (T3) Shallow-marine transgressive system tract deposition and associated generation of a transgressive ravinement surface (CR_{trs}) in marginal-erg regions.

© 2026 The Author(s). *Sedimentology* published by John Wiley & Sons Ltd on behalf of International Association of Sedimentologists, *Sedimentology*, **73**, 2081–2119

13653091, 2026, 6, Downloaded from https://onlinelibrary.wiley.com/doi/10.1111/sed.70126 by British Geological Survey, Wiley Online Library on [15/10/2026]. See the Terms and Conditions (https://onlinelibrary.wiley.com/terms-and-conditions) on Wiley Online Library for rules of use; OA articles are governed by the applicable Creative Commons License

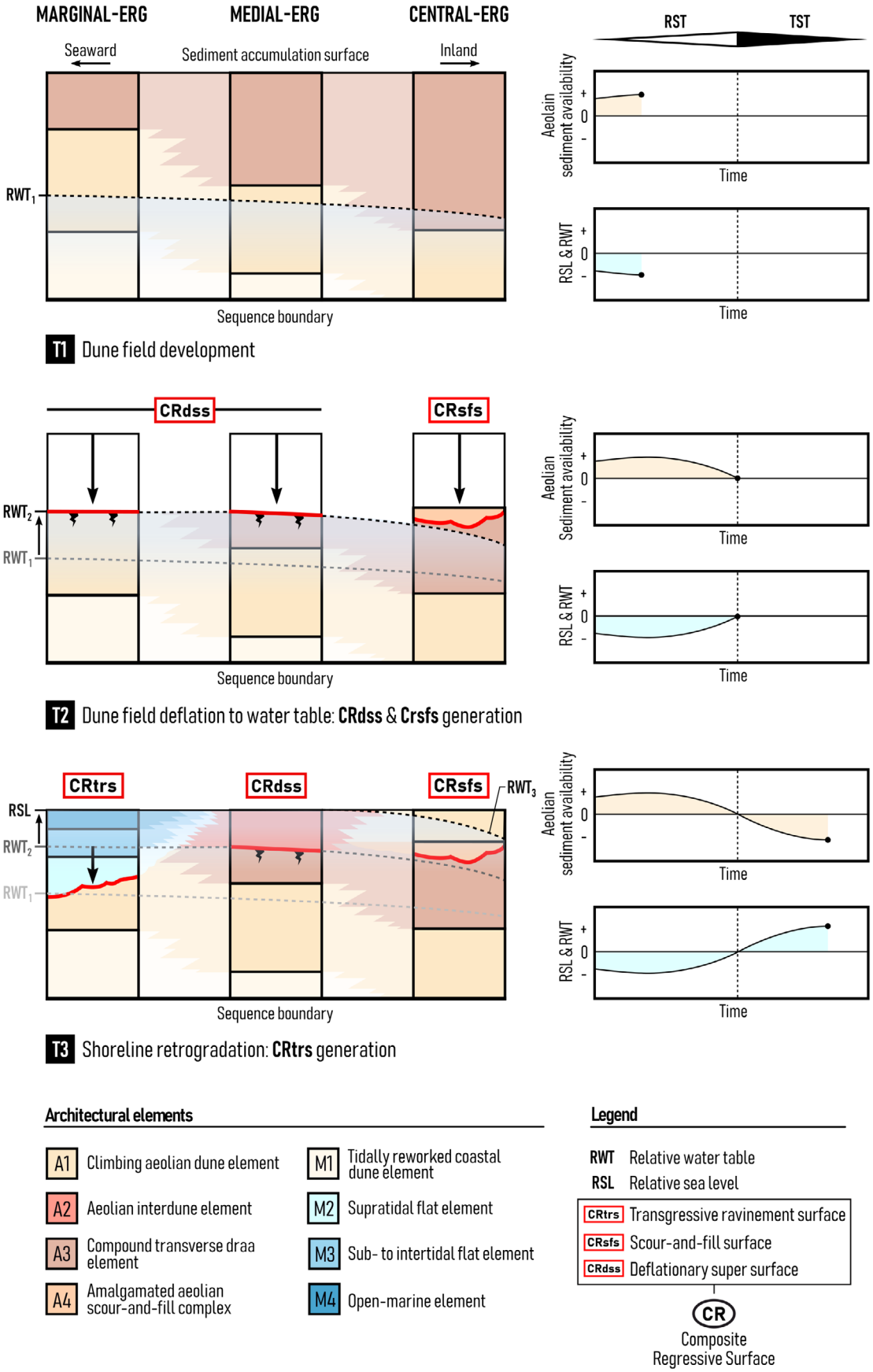

13653091, 2026, 6, Downloaded from https://onlinelibrary.wiley.com/doi/10.1111/sed.70126 by British Geological Survey, Wiley Online Library on [15/10/2026]. See the Terms and Conditions (https://onlinelibrary.wiley.com/terms-and-conditions) on Wiley Online Library for rules of use; OA articles are governed by the applicable Creative Commons License

sourced from contemporaneous marine realms. Coastal aeolian systems can be subdivided into depositional belts characterised by specific proportions of preserved sedimentary architectures: (i) central-erg, (ii) medial-erg and (iii) marginal-erg. Central-erg regions are dominated by the migration and climb of compound aeolian bedforms characteristic of high sediment availability conditions. Seaward declines in sediment availability translate into decreasing aeolian bedform complexity and crest-line sinuosity. Medial-erg regions are dominated by the migration of simple transverse dunes trains preserved in the form of climbing aeolian dune and interdune elements. Marginal-erg regions are the scene of complex process interplays between aeolian sediment drift, localised evaporitic precipitation and tidal currents. Their sedimentary record is characterised by discontinuous and heterogeneous coastal dune elements interbedded with supratidal strata deposited under periods of partial deflation.

The onset of transgressive system tracts generates diastemic transgressive ravinement surfaces onto which are deposited shallow-marine packages reworking parts of preceding erg-building sequences. In this scenario, reduced inland aeolian sediment availability results in the development of regional deflationary super surfaces and the preservation of aggrading sheet-like interdune elements (i.e. continental sabkhas) controlled by rates of relative water table rise. Amalgamated aeolian scour-and-fill complexes may be preserved in central-most regions of the erg where favourable sediment availability and accommodation conditions are sustained.

Spatial distributions of architectural elements recognised in the aeolian sequences of the Temple Cap Formation and the Page Sandstone are indicative of a coastal erg margin experiencing seaward changes in boundary conditions and surface processes ultimately leading to increasing stratigraphical heterogeneities towards their marine end-member. This study presents a novel model for the generation of aeolian sequences in response to relative sea-level fluctuations independently of their overarching allogenic controls. Accounting for the complex stratigraphical arrangements of such transitional systems and their spatial variability in architectural elements distribution can improve the characterisation of heterogeneities and compartmentalisation in equivalent subsurface reservoirs.

ACKNOWLEDGEMENTS

This research was conducted during a study undertaken as part of the Centre of Doctoral Training (CDT) in Geoscience and the Low Carbon Energy Transition (GeoNetZero). It is sponsored by Keele University and NeoEnergy Upstream, whose support is gratefully acknowledged. The authors thank the United States National Park Service for permitting this research and granting a scientific research permit for Dinosaur National Monument. The authors are grateful to Douglas Sprinkel for sharing his expertise on the geology of the San Rafael Group, Andrew Mitten and Oliver Button for their field assistance, as well as Don Hamilton for his precious technical support. We extend our gratitude to Jean-François Ghienne and an anonymous reviewer for providing very detailed and useful reports that significantly helped improving the quality of this article. Editors Jean-Yves Reynaud and Marcos Aurell are acknowledged for their dedicated support throughout the review process. Charlotte Priddy, Graham Leslie and Jack Heath are also thanked for their critical readings of an early version of this article. The authors declare that they have no conflict of interests.

DATA AVAILABILITY STATEMENT

The data that support the findings of this study are available from the corresponding author upon reasonable request.

REFERENCES

Abrantes, F.R., Jr., **Basilici, G.** and **Soares, M.V.T.** (2020) Mesoproterozoic erg and sand sheet system: architecture and controlling factors (Galho do Miguel Formation, SE Brazil). *Precambrian Res.*, **338**, 105592.

Ahmed Benan, C.A. and **Kocurek, G.** (2000) Catastrophic flooding of an aeolian dune field: Jurassic Entrada and Todilto Formations, Ghost Ranch, New Mexico, USA. *Sedimentology*, **47**, 1069–1080.

Al-Masrahy, M.A. and **Mountney, N.P.** (2013) Remote sensing of spatial variability in aeolian dune and interdune morphology in the Rub'Al-Khali, Saudi Arabia. *Aeol. Res.*, **11**, 155–170.

Alsharhan, A.S. and **Kendall, C.S.C.** (2003) Holocene coastal carbonates and evaporites of the southern Arabian Gulf and their ancient analogues. *Earth Sci. Rev.*, **61**, 191–243.

Andreason, M.W. (1992) Coastal siliciclastic sabkhas and related evaporative environments of the Permian Yates Formation, north Ward-Estes field, Ward County, Texas. *AAPG Bull.*, **76**, 1735–1759.

13653091, 2026, 6, Downloaded from https://onlinelibrary.wiley.com/doi/10.1111/sed.70126 by British Geological Survey, Wiley Online Library on [15/10/2026]. See the Terms and Conditions (https://onlinelibrary.wiley.com/terms-and-conditions) on Wiley Online Library for rules of use; OA articles are governed by the applicable Creative Commons License

Atchley, S.C. and **Loope, D.B.** (1993) Low-stand aeolian influence on stratigraphic completeness: upper member of the Hermosa formation (latest carboniferous), Southeast Utah, USA. In: *Aeolian Sediments: Ancient and Modern* (Eds Pye, K. and Lancaster, N.), 1st edn, pp. 127–149. The International Association of Sedimentologists, Gent.

Beveridge, C., **Kocurek, G.**, **Ewing, R.C.**, **Lancaster, N.**, **Morthekai, P.**, **Singhvi, A.K.** and **Mahan, S.A.** (2006) Development of spatially diverse and complex dune-field patterns: Gran Desierto Dune Field, Sonora, Mexico. *Sedimentology*, **53**, 1391–1409.

Bjerrum, C.J. and **Dorsey, R.J.** (1995) Tectonic controls on deposition of Middle Jurassic strata in a retroarc foreland basin, Utah-Idaho trough, western interior, United States. *Tectonics*, **14**, 962–978.

Blakey, R.C. (2014) Paleogeography and paleotectonics of the western interior seaway, Jurassic-Cretaceous of North America. *Search Discovery*, **30392**, 72.

Blakey, R.C., **Havholm, K.G.** and **Jones, L.S.** (1996) Stratigraphic analysis of eolian interactions with marine and fluvial deposits, Middle Jurassic Page Sandstone and Carmel Formation, Colorado Plateau, USA. *J. Sed. Res.*, **66**, 324–342.

Blakey, R.C. and **Middleton, L.T.** (1983) Permian shoreline eolian complex in central Arizona: dune changes in response to cyclic sealevel changes. In: *Developments in Sedimentology* (Eds Brookfield, M.E. and Ahlbrandt, T.S.), Vol. **38**, pp. 551–581. Elsevier, Amsterdam, Netherlands.

Blakey, R.C., **Peterson, F.**, **Caputo, M.V.**, **Geesaman, R.C.** and **Voorhees, B.J.** (1983) *Paleogeography of Middle Jurassic Continental, Shoreline, and Shallow Marine Sedimentation, Southern Utah*. Rocky Mountain Section (SEPM), Provo, UT.

Blakey, R.C., **Peterson, F.** and **Kocurek, G.** (1988) Synthesis of late Paleozoic and Mesozoic eolian deposits of the Western Interior of the United States. *Sed. Geol.*, **56**, 3–125.

Blanchard, S., **Fielding, C.R.**, **Frank, T.D.** and **Barrick, J.E.** (2016) Sequence stratigraphic framework for mixed aeolian, peritidal and marine environments: insights from the Pennsylvanian subtropical record of Western Pangaea. *Sedimentology*, **63**, 1929–1970.

Bofill, L., **Bozetti, G.**, **Schäfer, G.**, **Ghienne, J.-F.**, **Schuster, M.**, **Heap, M.J.**, **Knobelock, G.**, **Scherer, C.**, **Armenlenti, G.** and **de Souza, E.** (2025) Sedimentary control on permeability heterogeneity: the middle Buntsandstein continental sandstones (Lower Triassic, eastern France). *Mar. Petrol. Geol.*, **173**, 107261.

Bowler, B.J. (2026) *The sedimentology and variability of arid terminal fluvial fan systems: implications for reservoir characterisation*. MPhil Thesis, Keele University, Keele, UK.

Bromley, M. (1992) Topographic inversion of early interdune deposits, Navajo Sandstone (Lower Jurassic), Colorado Plateau, USA. *Sed. Geol.*, **80**, 1–25.

Brookfield, M.E. (1977) The origin of bounding surfaces in ancient aeolian sandstones. *Sedimentology*, **24**, 303–332.

Button, O., **Connor, J.G.**, **Pettigrew, R.P.**, **Kilhams, B.A.** and **Howell, J.A.** (2026) The regional evolution of a dryland Fluvio-aeolian and lacustrine succession in response to allocyclic forcing: insights from the Early Permian Cutler Group, Utah, USA. *Sedimentology*, **73**, 297–354.

Campos-Soto, S., **Benito, M.I.**, **Mountney, N.P.**, **Plink-Björklund, P.**, **Quijada, I.E.**, **Suarez-Gonzalez, P.** and **Cobos, A.** (2022) Where humid and arid meet: sedimentology of coastal siliciclastic successions deposited in apparently contrasting climates. *Sedimentology*, **69**, 975–1027.

Cardenas, B.T., **Kocurek, G.**, **Mohrig, D.**, **Swanson, T.**, **Hughes, C.M.** and **Brothers, S.C.** (2019) Preservation of autogenic processes and allogenic forcings in set-scale aeolian architecture II: the scour-and-fill dominated Jurassic Page Sandstone, Arizona, USA. *J. Sed. Res.*, **89**, 741–760.

Carr-Crabaugh, M. and **Dunn, T.L.** (1996) Reservoir heterogeneity as a function of accumulation and preservation dynamics. Tensleep Sandstone, Bighorn and Wind River basins, Wyoming. Rocky Mountain Section (SEPM), Paleozoic Systems of the Rocky Mountain Region, pp. 305–320.

Carr-Crabaugh, M. and **Kocurek, G.** (1998) Continental sequence stratigraphy of a wet eolian system: a key to relative sea-level change. In: *Relative Role of Eustacy, Climate, and Tectonism in Continental Rocks* (Ed Kocurek, G.). SEPM Special Publication, Tulsa, Oklahoma.

Chakrabarti, A. (2005) Sedimentary structures of tidal flats: a journey from coast to inner estuarine region of eastern India. *J. Earth Syst. Sci.*, **114**, 353–368.

Chan, M.A. (1989) Erg margin of the Permian White Rim Sandstone, SE Utah. *Sedimentology*, **36**, 235–251.

Chan, M.A. and **Kocurek, G.** (1988) Complexities in eolian and marine interactions: processes and eustatic controls on erg development. *Sed. Geol.*, **56**, 283–300.

Clement, A.M. and **Holland, S.M.** (2016) Sequence stratigraphic context of extensive basin-margin evaporites: middle Jurassic Gypsum Spring Formation, Wyoming, USA. *J. Sed. Res.*, **86**, 965–981.

Corbett, I. (1993) The modern and ancient pattern of sandflow through the southern Namib deflation basin. In: *Aeolian Sediments: Ancient and Modern* (Eds Pye, K. and Lancaster, N.), 1st edn, pp. 45–60. The International Association of Sedimentologists, Gent.

Cosgrove, G.I., **Colombera, L.** and **Mountney, N.P.** (2023) Quantitative analysis of aeolian stratigraphic architectures preserved in different tectonic settings. *Earth Sci. Rev.*, **237**, 104293.

Cosgrove, G.I.E., **Colombera, L.** and **Mountney, N.P.** (2022) The role of subsidence and accommodation generation in controlling the nature of the aeolian stratigraphic record. *J. Geol. Soc. Lond.*, **179**, jgs2021-042.

Cousins, D., **Kocurek, G.** and **Hern, C.** (2026) Methodological framework and evaluation of aeolian system sediment state: Wahiba Dune Field, Oman. *Sed. Geol.*, **497**, 107060.

Crabaugh, M. and **Kocurek, G.** (1993) Entrada sandstone: an example of a wet aeolian system. *Geol. Soc. London Spec. Publ.*, **72**, 103–126.

Cross, S., **Pettigrew, R.P.**, **Priddy, C.L.**, **Zuchuat, V.**, **Dodd, T.J.H.**, **Mitten, A.J.** and **Clarke, S.M.** (2023) The sedimentological expression of transgression–regression cycles upon aeolian–marine margins. *Depos. Rec.*, **9**, 335–362.

Currie, B.S. (1997) Sequence stratigraphy of nonmarine Jurassic–Cretaceous rocks, central Cordilleran foreland-basin system. *Geol. Soc. Am. Bull.*, **109**, 1206–1222.

Dalrymple, R.W. and **Rivers, J.M.** (2023) A new look at modern carbonate shoals and coastal barrier systems. *Earth-Sci. Rev.*, **246**, 104553.

Dickinson, W.R. and **Gehrels, G.E.** (2009) U-Pb ages of detrital zircons in Jurassic eolian and associated sandstones of the Colorado Plateau: evidence for

13653091, 2026, 6, Downloaded from https://onlinelibrary.wiley.com/doi/10.1111/sed.70126 by British Geological Survey, Wiley Online Library on [15/10/2026]. See the Terms and Conditions (https://onlinelibrary.wiley.com/terms-and-conditions) on Wiley Online Library for rules of use; OA articles are governed by the applicable Creative Commons License

transcontinental dispersal and intraregional recycling of sediment. *Geol. Soc. Am. Bull.*, **121**, 408–433.

Dickinson, W.R., **Stair, K.N.**, **Gehrels, G.E.**, **Peters, L.**, **Kowallis, B.J.**, **Blakey, R.C.**, **Amar, J.R.** and **Greenhalgh, B.W.** (2010) U-Pb and^{40} Ar/^{39} Ar ages for a tephra lens in the middle Jurassic page sandstone: first direct isotopic dating of a Mesozoic Eolianite on the Colorado plateau. *J. Geol.*, **118**, 215–221.

Doelling, H.H., **Sprinkel, D.A.**, **Kowallis, B.J.**, **Kuehne, P.A.**, **Morris, T.H.** and **Ressetar, R.** (2013) Temple Cap and Carmel Formations in the Henry Mountains Basin, Wayne and Garfield Counties, Utah. In: *The San Rafael Swell and Henry Mountains Basin—Geologic Centerpiece of Utah* (Eds Morris, T.H. and Ressetar, R.), Vol. **42**, pp. 279–318. Utah Geological Association Publication, Salt Lake City, UT.

Dott, R.H., **Byers, C.W.**, **Fielder, G.W.**, **Stenzel, S.R.** and **Winfree, K.E.** (1986) Aeolian to marine transition in Cambro—Ordovician cratonic sheet sandstones of the northern Mississippi valley, U.S.A. *Sedimentology*, **33**, 345–367.

Embry, A.F. (2010) Correlating siliciclastic successions with sequence stratigraphy. In: *Application of Modern Stratigraphic Techniques: Theory and Case Histories*, pp. 35–53. SEPM (Society for Sedimentary Geology), Tulsa, Oklahoma.

Eriksson, K.A. and **Truswell, J.F.** (1974) Tidal flat associations from a Lower Proterozoic carbonate sequence in South Africa. *Sedimentology*, **21**, 293–309.

Eschner, T.B. and **Kocurek, G.** (1986) Marine destruction of eolian sand seas; origin of mass flows. *J. Sed. Res.*, **56**, 401–411.

Ewing, R.C. and **Kocurek, G.A.** (2010) Aeolian dune interactions and dune-field pattern formation: white Sands Dune Field, New Mexico. *Sedimentology*, **57**, 1199–1219.

Falkenberg, P., **Vahrenkamp, S.**, **Garugleri, E.**, **Petrovic, A.**, **Hachmann, K.**, **Chandra, V.** and **Vahrenkamp, V.C.** (2025) Polygonal tepee structures of Arabia. *Depos. Rec.*, **12**, dep2.70043.

Ferronatto, J.P.F., **dos Santos Scherer, C.M.**, **de Souza, E.G.**, **dos Reis, A.D.** and **de Mello, R.G.** (2019) Genetic units and facies architecture of a Lower Cretaceous fluvial-aeolian succession, São Sebastião Formation, Jatobá Basin, Brazil. *J. S. Am. Earth Sci.*, **89**, 158–172.

Foote, N., **Hatter, S.J.**, **Gray, E.** and **Charlaftis, D.** (2025) Reservoir characterization of the Triassic Bunter Sandstone in the 43/28-NEPBH1 borehole: implications for CO_2 storage in the neighbouring Endurance structure, Southern North Sea, UK. *Geoenergy*, **3**, geoenergy2025-012.

Fryberger, S.G., **Al-Sari, A.M.** and **Clisham, T.J.** (1983) Eolian dune, interdune, sand sheet, and siliciclastic sabkha sediments of an offshore prograding sand sea, Dhahran area, Saudi Arabia. *AAPG Bull.*, **67**, 280–312.

Fryberger, S.G., **Krystinik, L.F.** and **Schenk, C.J.** (1990) Tidally flooded back-barrier dunefield, Guerrero Negro area, Baja California, Mexico. *Sedimentology*, **37**, 23–43.

Fryberger, S.G., **Schenk, C.J.** and **Krystinik, L.F.** (1988) Stokes surfaces and the effects of near-surface groundwater-table on aeolian deposition. *Sedimentology*, **35**, 21–41.

Gibling, M.R. (2006) Width and thickness of fluvial channel bodies and valley fills in the geological record: a literature compilation and classification. *J. Sed. Res.*, **76**, 731–770.

Gonzalez, R. and **Eberli, G.P.** (1997) Sediment transport and bedforms in a carbonate tidal inlet; Lee Stocking Island, Exumas, Bahamas. *Sedimentology*, **44**, 1015–1030.

Grantham, M. (2025) *High resolution, spatial and temporal evolution of a preserved coastal dune system, and its CCS implications*. MPhil Thesis, Keele University, Keele, UK.

Gross, E.C., **Carr, M.** and **Jobe, Z.R.** (2023) Three-dimensional bounding surface architecture and lateral facies heterogeneity of a wet aeolian system: Entrada Sandstone, Utah. *Sedimentology*, **70**, 145–178.

Hallam, A. (1985) A review of Mesozoic climates. *J. Geol. Soc.*, **142**, 433–445.

Havholm, K.G., **Blakey, R.C.**, **Capps, M.**, **Jones, L.S.**, **King, D.D.** and **Kocurek, G.** (1993) Aeolian genetic stratigraphy: an example from the middle Jurassic Page Sandstone, Colorado plateau. In: *Aeolian Sediments: Ancient and Modern*, 1st edn, pp. 85–107. The International Association of Sedimentologists, Gent.

Havholm, K.G. and **Kocurek, G.** (1994) Factors controlling aeolian sequence stratigraphy: clues from super bounding surface features in the Middle Jurassic Page Sandstone. *Sedimentology*, **41**, 913–934.

Hême de Lacotte, V.J.P., **Davies, C.H.C.**, **Bowler, B.J.**, **Clarke, S.M.**, **Leslie, A.G.** and **Sprinkel, D.A.** (2026) Facies mosaic distribution and stratigraphic disorder of a mixed carbonate–siliciclastic tidal succession. *Sedimentology*, **73**, sed.70048.

Hintze, L.F., **Willis, G.C.**, **Laes, D.Y.**, **Sprinkel, D.A.** and **Brown, K.D.** (2000) *Digital geologic map of Utah*. Utah Geological Survey, Utah.

Howell, J. and **Mountney, N.** (1997) Climatic cyclicity and accommodation space in arid to semi-arid depositional systems: an example from the Rotliegend Group of the UK southern North Sea. *Spec. Publ.*, **123**, 63–86.

Hunter, R.E. (1977) Basic types of stratification in small eolian dunes. *Sedimentology*, **24**, 361–387.

Inman, D.L., **Ewing, G.C.** and **Corliss, J.B.** (1966) Coastal sand dunes of Guerrero Negro, Baja California, Mexico. *Geol. Soc. Am. Bull.*, **77**, 787–802.

Issautier, B., **Fillacier, S.**, **Le Gallo, Y.**, **Audigane, P.**, **Chiaberge, C.** and **Viseur, S.** (2013) Modelling of CO_2 injection in fluvial sedimentary heterogeneous reservoirs to assess the impact of geological heterogeneities on CO2 storage capacity and performance. *Energy Procedia*, **37**, 5181–5190.

Jones, L.S. and **Blakey, R.C.** (1993) Erosional remnants and adjacent unconformities along an eolian-marine boundary of the Page Sandstone and Carmel Formation, Middle Jurassic, south-central Utah. *J. Sed. Res.*, **63**, 852–859.

Jones, L.S. and **Blakey, R.C.** (1997) Eolian-fluvial interaction in the Page Sandstone (Middle Jurassic) in south-central Utah, USA—a case study of erg-margin processes. *Sed. Geol.*, **109**, 181–198.

Jordan, O.D. and **Mountney, N.P.** (2010) Styles of interaction between aeolian, fluvial and shallow marine environments in the Pennsylvanian to Permian lower Cutler beds, south-east Utah, USA. *Sedimentology*, **57**, 1357–1385.

Jordan, O.D. and **Mountney, N.P.** (2012) Sequence stratigraphic evolution and cyclicity of an ancient coastal desert system: the Pennsylvanian–Permian Lower Cutler Beds, Paradox Basin, Utah, USA. *J. Sed. Res.*, **82**, 755–780.

Kamola, D.L. and **Chan, M.A.** (1988) Coastal dune facies, Permian Cutler Formation (White Rim Sandstone), Capitol Reef National Park area, southern Utah. *Sed. Geol.*, **56**, 341–356.

Kendall, A.C. (1978) Facies models 11. Continental and supratidal (sabkha) evaporites. *Geosci. Can.*, **5**, 66–78.

13653091, 2026, 6, Downloaded from https://onlinelibrary.wiley.com/doi/10.1111/sed.70126 by British Geological Survey, Wiley Online Library on [15/10/2026]. See the Terms and Conditions (https://onlinelibrary.wiley.com/terms-and-conditions) on Wiley Online Library for rules of use; OA articles are governed by the applicable Creative Commons License

Kinsman, D.J. (1969) Modes of formation, sedimentary associations, and diagnostic features of shallow-water and supratidal evaporites. *AAPG Bull.*, **53**, 830–840.

Kirkham, A. (1997) Shoreline evolution, aeolian deflation and anhydrite distribution of the Holocene, Abu Dhabi. *GeoArabia*, **2**, 403–416.

Kocurek, G. (1981) Significance of interdune deposits and bounding surfaces in aeolian dune sands. *Sedimentology*, **28**, 753–780.

Kocurek, G. (1988) First-order and super bounding surfaces in eolian sequences—bounding surfaces revisited. *Sed. Geol.*, **56**, 193–206.

Kocurek, G. and **Day, M.** (2018) What is preserved in the aeolian rock record? A Jurassic Entrada Sandstone case study at the Utah–Arizona border. *Sedimentology*, **65**, 1301–1321.

Kocurek, G. and **Dott, R.H.** (1981) Distinctions and uses of stratification types in the interpretation of eolian sand. *J. Sed. Res.*, **51**, 579–595.

Kocurek, G. and **Dott, R.H.** (1983) *Jurassic Paleogeography and Paleoclimate of the Central and Southern Rocky Mountains Region*. Rocky Mountain Section (SEPM), Provo, UT.

Kocurek, G. and **Ewing, R.C.** (2005) Aeolian dune field self-organization–implications for the formation of simple versus complex dune-field patterns. *Geomorphology*, **72**, 94–105.

Kocurek, G., **Ewing, R.C.** and **Mohrig, D.** (2010) How do bedform patterns arise? New views on the role of bedform interactions within a set of boundary conditions. *Earth Surf. Proc. Land.*, **35**, 51–63.

Kocurek, G. and **Fielder, G.** (1982) Adhesion structures. *J. Sed. Res.*, **52**, 1229–1241.

Kocurek, G. and **Havholm, K.G.** (1993) Eolian sequence stratigraphy—A conceptual framework. In: *Siliciclastic Sequence Stratigraphy: recent Developments and Applications* (Eds Weimer, P. and Posamentier, H.), Vol. **58**, p. 0. American Association of Petroleum Geologists, Tulsa, OK.

Kocurek, G., **Havholm, K.G.**, **Deynoux, M.** and **Blakey, R.C.** (1991) Amalgamated accumulations resulting from climatic and eustatic changes, Akchar Erg, Mauritania. *Sedimentology*, **38**, 751–772.

Kocurek, G. and **Hunter, R.E.** (1986) Origin of polygonal fractures in sand, uppermost Navajo and Page Sandstones, Page, Arizona. *J. Sed. Res.*, **56**, 895–904.

Kocurek, G., **Martindale, R.C.**, **Day, M.**, **Goudge, T.A.**, **Kerans, C.**, **Hassenruck-Gudipati, H.J.**, **Mason, J.**, **Cardenas, B.T.**, **Petersen, E.I.**, **Mohrig, D.**, **Aylward, D.S.**, **Hughes, C.M.** and **Nazworth, C.M.** (2019) Antecedent aeolian dune topographic control on carbonate and evaporite facies: Middle Jurassic Todilto Member, Wanakah Formation, Ghost Ranch, New Mexico, USA. *Sedimentology*, **66**, 808–837.

Kocurek, G., **Robinson, N.I.** and **Sharp, J.M., Jr.** (2001) The response of the water table in coastal aeolian systems to changes in sea level. *Sed. Geol.*, **139**, 1–13.

Kocurek, G., **Townsley, M.**, **Yeh, E.**, **Havholm, K.G.** and **Sweet, M.L.** (1992) Dune and dune-field development on Padre Island, Texas, with implications for interdune deposition and water-table-controlled accumulation. *J. Sed. Res.*, **62**, 622–635.

Kowallis, B.J., **Christiansen, E.H.**, **Deino, A.L.**, **Zhang, C.** and **Everett, B.H.** (2001) The record of Middle Jurassic volcanism in the Carmel and Temple Cap Formations of southwestern Utah. *GSA Bull.*, **113**, 373–387.

Langford, R.P. and **Chan, M.A.** (1988) Flood surfaces and deflation surfaces within the Cutler Formation and Cedar Mesa Sandstone (Permian), southeastern Utah. *Geol. Soc. Am. Bull.*, **100**, 1541–1549.

Lokier, S.W. (2012) Development and evolution of subaerial halite crust morphologies in a coastal sabkha setting. *J. Arid Environ.*, **79**, 32–47.

Loope, D.B. (1985) Episodic deposition and preservation of eolian sands: a late Paleozoic example from southeastern Utah. *Geology*, **13**, 73–76.

Loope, D.B. (1988) Rhizoliths in ancient eolianites. *Sed. Geol.*, **56**, 301–314.

Loope, D.B., **Rowe, C.M.** and **Joeckel, R.M.** (2001) Annual monsoon rains recorded by Jurassic dunes. *Nature*, **412**, 64–66.

Marzolf, J.E. (1991) Lower Jurassic unconformity (J-0) from the Colorado Plateau to the eastern Mojave Desert: evidence of a major tectonic event at the close of the Triassic. *Geology*, **19**, 320–323.

McCubbin, D.G. (1982) Barrier-island and strand-plain facies. AAPG Special Volumes, Sandstone Depositional Environments, pp. 247–279.

McKay, C.P., **Rask, J.C.**, **Detweiler, A.M.**, **Bebout, B.M.**, **Everroad, R.C.**, **Lee, J.Z.**, **Chanton, J.P.**, **Mayer, M.H.**, **Caraballo, A.A.** and **Kapili, B.** (2016) An unusual inverted saline microbial mat community in an interdune sabkha in the Rub'al Khali (the Empty Quarter), United Arab Emirates. *PLoS One*, **11**, e0150342.

Melnyk, S., **Birgenheier, L.P.**, **Vanden Berg, M.D.**, **ST. Pierre, G.A.E.**, **Edelman, E.** and **Tankersley, T.** (2026) Sedimentological controls on reservoir heterogeneity in the eolian Entrada Sandstone: implications for geologic carbon storage. *Journal of Sedimentary Research*, **96**, 506–523. https://doi.org/10.2110/jsr.2025.047

Mesquita, Á.F., **Basilici, G.**, **Soares, M.V.T.** and **Garcia, R.G.V.** (2021) Morphology, accumulation and preservation of draa systems in a Precambrian erg (Galho do Miguel Formation, SE Brazil). *Sed. Geol.*, **412**, 105807.

Mountney, N., **Howell, J.**, **Flint, S.** and **Jerram, D.** (1999) Relating eolian bounding-surface geometries to the bed forms that generated them: Etjo Formation, Cretaceous, Namibia. *Geology*, **27**, 159–162.

Mountney, N.P. (2006) Periodic accumulation and destruction of aeolian erg sequences in the Permian Cedar Mesa Sandstone, White Canyon, southern Utah, USA. *Sedimentology*, **53**, 789–823.

Mountney, N.P. (2012) A stratigraphic model to account for complexity in aeolian dune and interdune successions. *Sedimentology*, **59**, 964–989.

Mountney, N.P. and **Howell, J.** (2000) Aeolian architecture, bedform climbing and preservation space in the Cretaceous Etjo Formation, NW Namibia. *Sedimentology*, **47**, 825–849.

Mountney, N.P. and **Jagger, A.** (2004) Stratigraphic evolution of an aeolian erg margin system: the Permian Cedar Mesa Sandstone, SE Utah, USA. *Sedimentology*, **51**, 713–743.

Mountney, N.P. and **Thompson, D.B.** (2002) Stratigraphic evolution and preservation of aeolian dune and damp/wet interdune strata: an example from the Triassic Helsby Sandstone Formation, Cheshire Basin, UK. *Sedimentology*, **49**, 805–833.

Olariu, C., **Steel, R.J.**, **Dalrymple, R.W.** and **Gingras, M.K.** (2012) Tidal dunes versus tidal bars: the sedimentological and architectural characteristics of compound dunes in a

13653091, 2026, 6, Downloaded from https://onlinelibrary.wiley.com/doi/10.1111/sed.70126 by British Geological Survey, Wiley Online Library on [15/10/2026]. See the Terms and Conditions (https://onlinelibrary.wiley.com/terms-and-conditions) on Wiley Online Library for rules of use; OA articles are governed by the applicable Creative Commons License

tidal seaway, the lower Baronia Sandstone (Lower Eocene), Ager Basin, Spain. *Sed. Geol.*, **279**, 134–155.

Parrish, J.T. and **Peterson, F.** (1988) Wind directions predicted from global circulation models and wind directions determined from eolian sandstones of the western United States—A comparison. *Sed. Geol.*, **56**, 261–282.

Paz, M., **Ponce, J.J.**, **Mángano, M.G.**, **Buatois, L.A.**, **Carmona, N.B.**, **Wetzel, A.**, **Pereira, E.** and **Rodríguez, M.N.** (2021) The Vaca Muerta transgression (Upper Jurassic), Neuquén Basin, Argentina: insights into the evolution and timing of aeolian–marine transitions. *Sedimentology*, **68**, 2732–2764.

Peterson, F. (1988) Pennsylvanian to Jurassic eolian transportation systems in the western United States. *Sed. Geol.*, **56**, 207–260.

Pettigrew, R.P., **Priddy, C.**, **Clarke, S.M.**, **Warke, M.R.**, **Stüeken, E.E.** and **Claire, M.W.** (2021) Sedimentology and isotope geochemistry of transitional evaporitic environments within arid continental settings: from erg to saline lakes. *Sedimentology*, **68**, 907–942.

Pettigrew, R.P., **Priddy, C.L.** and **Clarke, S.M.** (2024) Outcrop spectral gamma-ray signals of distal arid continental basins: Facies identification and controls. *Mar. Pet. Geol.*, **168**, 107047.

Phillips, J.D., **Ewing, R.C.**, **Bowling, R.**, **Weymer, B.A.**, **Barrineau, P.**, **Nittrouer, J.A.** and **Everett, M.E.** (2019) Low-angle eolian deposits formed by protodune migration, and insights into slipface development at White Sands Dune Field, New Mexico. *Aeol. Res.*, **36**, 9–26.

Picard, M.D. and **Uygur, K.** (1982) Mixed terrigenous-carbonate rocks in Jurassic Arapien Shale of central Utah. *Utah Geol. Assoc. Publ.*, **10**, 181–198.

Pipiringos, G.N. and **O'Sullivan, R.B.** (1978) *Principal Unconformities in Triassic and Jurassic Rocks, Western Interior United States – A Preliminary Survey*. United States Government Printing Office, Washington, DC.

Polo, C.A., **Melvin, J.**, **Hooker, N.P.**, **Rees, A.J.**, **Gingras, M.K.** and **Pemberton, S.G.** (2020) Ichnology and sedimentology of aeolian and shallow-marine interactions in the Permian Unayzah Group of central Saudi Arabia: towards a mechanism for infaunal colonization of coastal dune fields and erg margins. *Sedimentology*, **67**, 1797–1843.

Priddy, C.L. and **Clarke, S.M.** (2020) The sedimentology of an ephemeral fluvial–aeolian succession. *Sedimentology*, **67**, 2392–2425.

Priddy, C.L., **Pettigrew, R.P.**, **Watson, D.**, **Regis, A.V.** and **Clarke, S.M.** (2023) Aeolian–lacustrine margins: implications for carbon capture and storage within the Rotliegend Group, Southern North Sea. *Geoenergy*, **1**. https://doi.org/10.1144/geoenergy2023-031.

Reineck, H. and **Wunderlich, F.** (1968) Classiffication and origin of flaser and lenticular bedding. *Sedimentology*, **11**, 99–104.

Riding, R. and **Wright, V.P.** (1981) Paleosols and tidal-flat/lagoon sequences on a carboniferous carbonate shelf; sedimentary associations of triple disconformities. *J. Sed. Res.*, **51**, 1323–1339.

Rivers, J.M., **Dalrymple, R.W.**, **Yousif, R.**, **Al-Shaikh, I.**, **Butler, J.D.**, **Warren, C.**, **Skeat, S.L.** and **Bari, E.M.A.** (2020) Mixed siliciclastic-carbonate-evaporite sedimentation in an arid eolian landscape: the Khor Al Adaid tide-dominated coastal embayment, Qatar. *Sed. Geol.*, **408**, 105730.

Roberts, A.L., **Gupta, S.**, **Banham, S.G.**, **Cowart, A.**, **Edgar, L.A.**, **Rapin, W.**, **Dietrich, W.E.**, **Davis, J.M.**, **Kite, E.S.**, **Caravaca, G.**, **Mondro, C.A.**, **Gasda, P.J.**, **Johnson, J.R.**, **Le Mouélic, S.**, **Fey, D.M.**, **Bryk, A.B.**, **Paar, G.**, **Harris, E.R.A.**, **Fraeman, A.** and **Vasavada, A.R.** (2025) Paleoscours within the layered sulfate-bearing unit at Gale Crater, Mars: evidence for intense wind erosion. *J. Geophys. Res. Planets*, **130**, e2024JE008680.

Roca, X. and **Nadon, G.C.** (2007) Tectonic control on the sequence stratigraphy of nonmarine retroarc foreland basin fills: insights from the Upper Jurassic of central Utah, USA. *J. Sed. Res.*, **77**, 239–255.

Rodríguez-López, J.P., **Meléndez, N.**, **De Boer, P.L.** and **Soria, A.R.** (2010) The action of wind and water in a mid-Cretaceous subtropical erg-margin system close to the Variscan Iberian Massif, Spain. *Sedimentology*, **57**, 1315–1356.

Rodríguez-López, J.P., **Meléndez, N.**, **De Boer, P.L.** and **Soria, A.R.** (2012) Controls on marine–erg margin cycle variability: aeolian–marine interaction in the mid-Cretaceous Iberian Desert System, Spain. *Sedimentology*, **59**, 466–501.

Rodríguez-López, J.P., **Meléndez, N.**, **de Boer, P.L.**, **Soria, A.R.** and **Liesa, C.L.** (2013) Spatial variability of multi-controlled aeolian supersurfaces in central-erg and marine-erg-margin systems. *Aeol. Res.*, **11**, 141–154.

Rubin, D.M. and **Hunter, R.E.** (1982) Bedform climbing in theory and nature. *Sedimentology*, **29**, 121–138.

Rubin, D.M. and **Hunter, R.E.** (1983) Reconstructing bedform assemblages from compound crossbedding. In: *Developments in Sedimentology*, Vol. **38**, pp. 407–427. Elsevier, Amsterdam, Netherlands.

Schumm, S.A. (1993) River response to baselevel change: implications for sequence stratigraphy. *J. Geol.*, **101**, 279–294.

Shanley, K.W. and **McCabe, P.J.** (1994) Perspectives on the sequence stratigraphy of continental strata. *AAPG Bull.*, **78**, 544–568.

Sohal, M.A., **Le Gallo, Y.**, **Audigane, P.**, **De Dios, J.C.** and **Rigby, S.P.** (2021) Effect of geological heterogeneities on reservoir storage capacity and migration of CO_2 plume in a deep saline fractured carbonate aquifer. *Int. J. Greenh. Gas Con.*, **108**, 103306.

Sprinkel, D., **Doelling, H.H.**, **Kowallis, B.J.**, **Waanders, G.** and **Kuehne, P.A.** (2024) Stratigraphy, correlation, and age of the Gypsum Spring, Temple Cap, Arapien, Carmel, and Twin Creek Formations (Early and Middle Jurassic) of Utah and surrounding states. *Utah Geol. Surv. Contract Deliv.*, **18**, 220.

Sprinkel, D.A. (1982) Twin Creek Limestone-Arapien Shale relations in central Utah.

Sprinkel, D.A., **Doelling, H.H.**, **Kowallis, B.J.**, **Waanders, G.**, **Kuehne, P.A.**, **Yonkee, W.A.** and **Chidsey, T.C.** (2011) Early results of a study of Middle Jurassic strata in the Sevier fold and thrust belt, Utah. In: *Sevier Thrust Belt—Northern and Central Utah and Adjacent Areas* (Eds Sprinkel, D.A., Yonkee, W.A. and Chidsey, T.C., Jr.), Vol. **40**, pp. 151–172. Utah Geological Association Publication, Salt Lake City, UT.

Steel, R.J., **Plink-Bjorklund, P.** and **Aschoff, J.** (2012) Tidal deposits of the Campanian Western Interior Seaway, Wyoming, Utah and Colorado, USA. In: *Principles of Tidal Sedimentology* (Eds Davis, R.A. and Dalrymple, R.W.), pp. 437–471. Springer Netherlands, Dordrecht.

Stokes, W.L. (1968) Multiple parallel-truncation bedding planes; a feature of wind-deposited sandstone formations. *J. Sed. Res.*, **38**, 510–515.

13653091, 2026, 6, Downloaded from https://onlinelibrary.wiley.com/doi/10.1111/sed.70126 by British Geological Survey, Wiley Online Library on [15/10/2026]. See the Terms and Conditions (https://onlinelibrary.wiley.com/terms-and-conditions) on Wiley Online Library for rules of use; OA articles are governed by the applicable Creative Commons License

Strömbäck, A., **Howell, J.A.** and **Veiga, G.D.** (2005) The transgression of an erg–sedimentation and reworking/soft-sediment deformation of aeolian facies: the Cretaceous Troncoso Member, Neuquén Basin, Argentina.

Suarez-Gonzalez, P., **Benito, M.I.**, **Quijada, I.E.**, **Mas, R.** and **Campos-Soto, S.** (2019) 'Trapping and binding': a review of the factors controlling the development of fossil agglutinated microbialites and their distribution in space and time. *Earth-Sci. Rev.*, **194**, 182–215.

Swanson, T., **Mohrig, D.**, **Kocurek, G.**, **Cardenas, B.T.** and **Wolinsky, M.A.** (2019) Preservation of autogenic processes and allogenic forcings in set-scale aeolian architecture I: numerical experiments. *J. Sed. Res.*, **89**, 728–740.

Taggart, S., **Hampson, G.J.** and **Jackson, M.D.** (2010) High-resolution stratigraphic architecture and lithological heterogeneity within marginal aeolian reservoir analogues. *Sedimentology*, **57**, 1246–1279.

Taylor, A.M. and **Goldring, R.** (1993) Description and analysis of bioturbation and ichnofabric. *J. Geol. Soc.*, **150**, 141–148.

Thorman, C.H. (2011) The Elko orogeny–A major tectonic event in eastern Nevada–western Utah. In: *Sevier Thrust Belt: Northern and Central Utah and Adjacent Areas* (Eds Sprinkel, D.A., Yonkee, W.A. and Chidsey, T.C., Jr.), Vol. **40**, pp. 117–129. Utah Geological Association Publication, Salt Lake City, UT.

Veiga, G.D., **Howell, J.A.** and **Strömbäck, A.** (2005) Anatomy of a mixed marine–non-marine lowstand wedge in a ramp setting. The record of a Barremian–Aptian Complex Relative Sea-Level Fall in the Central Neuquén Basin, Argentina. In: *The Neuquén Basin, Argentina: A Case Study in Sequence Stratigraphy and Basin Dynamics* (Eds Veiga, G.D., Spalletti, L.A., Howell, J.A. and Schwarz, E.), Vol. **252**. Geological Society, London, Special Publications, London, UK.

Vieira, L.V. and **dos Santos Scherer, C.M.** (2017) Facies architecture and high resolution sequence stratigraphy of an aeolian, fluvial and shallow marine system in the Pennsylvanian Piauí Formation, Parnaíba Basin, Brazil. *J. S. Am. Earth Sci.*, **76**, 238–256.

Wood, G.V. and **Wolfe, M.J.** (1969) Sabkha cycles in the Arab/Darb formation off the Trucial Coast of Arabia. *Sedimentology*, **12**, 165–191.

Zuchuat, V., **Midtkandal, I.**, **Poyatos-Moré, M.**, **Da Costa, S.**, **Brooks, H.L.**, **Halvorsen, K.**, **Cote, N.**, **Sundal, A.** and **Braathen, A.** (2019b) Composite and diachronous stratigraphic surfaces in low-gradient, transitional settings: the J-3 "unconformity" and the Curtis Formation, east-central Utah, U.S.A. *J. Sed. Res.*, **89**, 1075–1095.

Zuchuat, V., **Sleveland, A.R.N.**, **Pettigrew, R.P.**, **Dodd, T.J.H.**, **Clarke, S.M.**, **Rabbel, O.**, **Braathen, A.** and **Midtkandal, I.** (2019a) Overprinted allocyclic processes by tidal resonance in an epicontinental basin: the Upper Jurassic Curtis Formation, east-central Utah, USA. *Depos. Rec.*, **5**, 272–305.

Manuscript received 13 December 2025; revision accepted 28 May 2026

© 2026 The Author(s). *Sedimentology* published by John Wiley & Sons Ltd on behalf of International Association of Sedimentologists, *Sedimentology*, **73**, 2081–2119

13653091, 2026, 6, Downloaded from https://onlinelibrary.wiley.com/doi/10.1111/sed.70126 by British Geological Survey, Wiley Online Library on [15/10/2026]. See the Terms and Conditions (https://onlinelibrary.wiley.com/terms-and-conditions) on Wiley Online Library for rules of use; OA articles are governed by the applicable Creative Commons License